

## Article

# Mutational Activation of the NRF2 Pathway Upregulates Kynureninase Resulting in Tumor Immunosuppression and Poor Outcome in Lung Adenocarcinoma

Johannes F. Fahrman<sup>1</sup>, Ichidai Tanaka<sup>2</sup>, Ehsan Irajizad<sup>3</sup>, Xiangying Mao<sup>1</sup>, Jennifer B. Dennison<sup>1</sup>, Eunice Murage<sup>1</sup>, Julian Casabar<sup>1</sup>, Jeffrey Mayo<sup>4</sup>, Qian Peng<sup>4</sup>, Muge Celiktas<sup>1</sup>, Jody V. Vykoukal<sup>1</sup>, Soyoung Park<sup>1</sup>, Ayumu Taguchi<sup>5</sup>, Oliver Delgado<sup>1</sup>, Satyendra C. Tripathi<sup>6</sup>, Hiroyuki Katayama<sup>1</sup>, Luisa Maren Solis Soto<sup>7</sup>, Jaime Rodriguez-Canales<sup>7</sup>, Carmen Behrens<sup>7</sup>, Ignacio Wistuba<sup>7</sup>, Samir Hanash<sup>1</sup> and Edwin J. Ostrin<sup>4,\*</sup>

- <sup>1</sup> Department of Clinical Cancer Prevention, The University of Texas MD Anderson Cancer Center, 1515 Holcombe Blvd., Houston, TX 77030, USA; jffahrman@mdanderson.org (J.F.F.); xmao2@mdanderson.org (X.M.); jbdennis@mdanderson.org (J.B.D.); enmurage@mdanderson.org (E.M.); jpcasabar@mdanderson.org (J.C.); mceliktas@mdanderson.org (M.C.); jvykouka@mdanderson.org (J.V.V.); snpark@mdanderson.org (S.P.); olidel8@gmail.com (O.D.); hkatayama1@mdanderson.org (H.K.); shanash@mdanderson.org (S.H.)
- <sup>2</sup> Department of Respiratory Medicine, Nagoya University Graduate School of Medicine, Nagoya 464-8601, Japan; ichidai@med.nagoya-u.ac.jp
- <sup>3</sup> Department of Biostatistics, The University of Texas MD Anderson Cancer Center, 1515 Holcombe Blvd., Houston, TX 77030, USA; eirajizad@mdanderson.org
- <sup>4</sup> Department of General Internal Medicine, The University of Texas MD Anderson Cancer Center, 1515 Holcombe Blvd., Houston, TX 77030, USA; jmayo1@mdanderson.org (J.M.); qpeng@mdanderson.org (Q.P.)
- <sup>5</sup> Division of Molecular Diagnostics, Aichi Cancer Center, Kanokoden, Chikusa-ku, Nagoya 464-8681, Japan; a.taguchi@aichi-cc.jp
- <sup>6</sup> All India Institute of Medicine Sciences, Nagpur 441108, India; sctripathi@aiimsnagpur.edu.in
- <sup>7</sup> Department of Translational Molecular Pathology, The University of Texas MD Anderson Cancer Center, 1515 Holcombe Blvd., Houston, TX 77030, USA; lmsolis@mdanderson.org (L.M.S.S.); rodriga2@gmail.com (J.R.-C.); cbehrens@mdanderson.org (C.B.); iiwistuba@mdanderson.org (I.W.)
- \* Correspondence: ejostrin@mdanderson.org; Tel.: +713-792-5389; Fax: +713-563-5746



**Citation:** Fahrman, J.F.; Tanaka, I.; Irajizad, E.; Mao, X.; Dennison, J.B.; Murage, E.; Casabar, J.; Mayo, J.; Peng, Q.; Celiktas, M.; et al. Mutational Activation of the NRF2 Pathway Upregulates Kynureninase Resulting in Tumor Immunosuppression and Poor Outcome in Lung Adenocarcinoma. *Cancers* **2022**, *14*, 2543. <https://doi.org/10.3390/cancers14102543>

Academic Editor: Atsushi Umemura

Received: 15 April 2022

Accepted: 17 May 2022

Published: 21 May 2022

**Publisher's Note:** MDPI stays neutral with regard to jurisdictional claims in published maps and institutional affiliations.



**Copyright:** © 2022 by the authors. Licensee MDPI, Basel, Switzerland. This article is an open access article distributed under the terms and conditions of the Creative Commons Attribution (CC BY) license (<https://creativecommons.org/licenses/by/4.0/>).

**Simple Summary:** Activation of the Nuclear factor-erythroid factor 2-related factor 2 (NRF2) pathway through gain-of-function mutations or loss-of-function of its suppressor Kelch-like ECH-associated protein 1 (KEAP1) is frequent in lung cancer. NRF2 activation has also been reported to alter the tumor microenvironment. Proteomic profiles of 47 lung adenocarcinoma (LUAD) cell lines (11 *KEAP1* mutant and 36 *KEAP1* wild-type) revealed the tryptophan-kynurenine enzyme kynureninase (KYNU) as a top overexpressed protein associated with activated NRF2. Mechanistic studies demonstrated that NRF2 is a regulator of enzymatically functional KYNU in LUAD. Analysis of multiple independent gene expression datasets of human lung cancer and a LUAD tumor microarray demonstrated that elevated tumor KYNU expression was associated with immunosuppression, including potent induction of T-regulatory cells, increased levels of PD1 and PD-L1, and poorer overall survival. Our findings indicate a novel mechanism of NRF2 tumoral immunosuppression through upregulation of KYNU.

**Abstract:** Activation of the NRF2 pathway through gain-of-function mutations or loss-of-function of its suppressor KEAP1 is a frequent finding in lung cancer. NRF2 activation has been reported to alter the tumor microenvironment. Here, we demonstrated that NRF2 alters tryptophan metabolism through the kynurenine pathway that is associated with a tumor-promoting, immune suppressed microenvironment. Specifically, proteomic profiles of 47 lung adenocarcinoma (LUAD) cell lines (11 *KEAP1* mutant and 36 *KEAP1* wild-type) revealed the tryptophan-kynurenine enzyme kynureninase (KYNU) as a top overexpressed protein associated with activated NRF2. The siRNA-mediated knockdown of *NFE2L2*, the gene encoding for NRF2, or activation of the NRF2 pathway through

siRNA-mediated knockdown of *KEAP1* or via chemical induction with the NRF2-activator CDDO-Me confirmed that NRF2 is a regulator of KYNU expression in LUAD. Metabolomic analyses confirmed KYNU to be enzymatically functional. Analysis of multiple independent gene expression datasets of LUAD, as well as a LUAD tumor microarray demonstrated that elevated KYNU was associated with immunosuppression, including potent induction of T-regulatory cells, increased levels of PD1 and PD-L1, and resulted in poorer survival. Our findings indicate a novel mechanism of NRF2 tumoral immunosuppression through upregulation of KYNU.

**Keywords:** NRF2; KEAP1; lung adenocarcinoma; metabolism; kynurenine pathway; kynureninase; immune suppression; prognostic marker

## 1. Introduction

Activation of the nuclear factor erythroid 2-related factor 2 (NRF2) pathway, either through gain-of-function mutation or loss-of-function of its suppressor, Kelch-like ECH-associated protein 1 (KEAP1), is one of the most dysregulated pathways in lung adenocarcinoma (LUAD) [1,2]. NRF2 is a critical stress response mediator in mammalian cells. NRF2 is regulated by KEAP1, which binds the N-terminal Neh2 regulatory domain of NRF2, mediating its degradation via polyubiquitination and thereby inhibiting NRF2 nuclear translocation and subsequent target gene expression [3]. Nuclear translocation of NRF2 due to loss of KEAP1 expression by allelic inactivation of the gene via mutation, loss of heterozygosity or promoter methylation has been shown to frequently occur in *KRAS* mutant lung adenocarcinoma [2]. NRF2 regulates basal and inducible expression of hundreds of genes that contain antioxidant response elements (AREs) in their regulatory regions by heterodimerizing with small MAF proteins. NRF2-target genes are involved in multiple cellular pathways, including those that control reduction/oxidation (redox) homeostasis, drug metabolism and excretion, energetics, amino acid metabolism, iron metabolism, and mitochondrial physiology [4]. Activation of NRF2 has been associated with induction of chemoresistance and disease progression in several cancer types [5–11]. Recent evidence further demonstrates a pivotal role of NRF2 activation in modulating tumor metabolism and the tumor immunophenotype [12–15]. For example, NRF2 has been shown to regulate expression of key serine/glycine biosynthesis enzymes via activating transcription factor 4 (ATF4) to support glutathione and nucleotide production [15]. Prior studies have also shown that lung cancer cells harboring *KRAS* mutations reprograms cancer cell metabolite towards glutamine dependence through NRF2-mediated signaling activities that increase expression of enzymes involved in glutaminolysis [16–18]. Nevertheless, the extent to which NRF2 activation regulates tumor metabolism and how these changes impact tumor-immune interaction remains incomplete.

Here, we performed an initial screen of 47 lung adenocarcinoma (LUAD) cell lines to identify protein signatures related to *KEAP1* mutational status and activated NRF2, the results of which revealed the kynurenine-metabolizing enzyme kynureninase (KYNU) as a top differential overexpressed protein associated with activated NRF2. KYNU is a pyridoxal-5'-phosphate (pyridoxal-P)-dependent enzyme that catalyses the hydrolysis of kynurenine and 3-hydroxykynurenine into anthranilic and 3-hydroxyanthranilic acids, respectively. In mammalian cells, KYNU is involved in the biosynthesis of NAD cofactors from tryptophan through the kynurenine pathway [19]. Here, we show that the overexpression of KYNU was independent of induction of the entire tryptophan-kynurenine pathway (KP). We then evaluated the functional relevance of KYNU overexpression in LUAD and its impact on the tumor immunophenotype, showing marked immunomodulation towards a suppressive inflammatory infiltrate.

## 2. Materials and Methods

Detailed information regarding methodologies is provided in Appendix A.

### 2.1. Cell Culture and Transfection

Cancer cell lines were maintained in Roswell Park Memorial Institute (RPMI) media plus 10% fetal bovine serum (FBS) unless otherwise stated. Small interfering RNA (siRNA) transfection experiments were performed using the following siRNAs: siControl (Silencer Select Negative Control #1, Life Technologies, Carlsbad, CA, USA), siKYNU #1 and #2 (s17103 and s1704, Invitrogen, Waltham, MA, USA), siKEAP1 #1 and #2 (#00080908 and #00344034, Sigma Aldrich, St. Louis, MO, USA) and siNFE2L2 #1 and #2 (#00182393 and #00341015, Sigma Aldrich).

### 2.2. Chemicals

CDDO-Me (2-Cyano-3,12-dioxo-oleana-1,9(11)-dien-28-oic acid methyl, or bardoxolone methyl) was purchased from Sigma Aldrich. Stock solutions were resuspended in dimethyl sulfoxide (DMSO).

### 2.3. Western Blot Analysis

Primary antibodies include  $\alpha$ -KYNU (Santa Cruz Biotechnology, Dallas, TX, USA, sc-390360; 1:200 dilution),  $\alpha$ -IDO (Abcam, Cambridge, UK, ab55305; 1:500 dilution),  $\alpha$ -QPRT (Abcam, ab171944; 1:1000 dilution),  $\alpha$ -Nrf2 (Abcam, Cambridge, UK, ab62352; 1:500 dilution),  $\alpha$ -KEAP1 (ProteinTech, Rosemont, IL, USA, 10503-2-AP; 1:1000 dilution),  $\alpha$ -NQO1 (Abcam, Cambridge, UK, ab34173; 1:10,000 dilution),  $\alpha$ -Peroxisome oxidoreductin-1 (Abcam, Cambridge, UK, ab41906; 1:10,000 dilution), and  $\alpha$ -glutathione reductase (Abcam, Cambridge, UK, ab128933; 1:5000 dilution).  $\beta$ -Actin primary antibody (Sigma Aldrich, St. Louis, MO, USA; 1:5000 dilution) was used as a control for protein loading. Uncut blots are provided in Figure A1 in the Appendix B.

### 2.4. RT-PCR Analysis

RNA was extracted using the RNeasy Extraction Kit (Qiagen, Germantown, MD, USA) according to manufacturer's protocol. TaqMan PCR assay was performed with a 7500 Fast Real-Time PCR System using universal TaqMan PCR master mix (ThermoFisher, Waltham, MA, USA) and FAM<sup>TM</sup>-labeled probes for KYNU (Hs00187560\_m1) and KEAP1 (Hs00202227\_m1) and VIC<sup>TM</sup>-labeled probes for  $\beta$ 2M (Hs\_00187842\_m1). PCR was carried out using a BioRad CFX Connect RT System (Hercules, CA, USA). Values are reported as  $2^{-\Delta\Delta C_t}$ .

### 2.5. Proteomic Analysis

For proteomic analyses, each cancer cell line ( $n = 47$  cell lines) was analyzed as a singular replicate. For these experiments, cancer cell lines (Table A1) were grown for seven passages in RPMI-1640 supplemented with <sup>13</sup>C-lysine and 10% dialyzed FBS according to the standard SILAC protocol [20]. The purpose of SILAC labeling was to discriminate the FBS derived proteins which may affect the identification of the cell surface protein list.

### 2.6. Metabolomic Analysis

#### 2.6.1. Exometabolome Experiments

Exometabolome experiments were performed on conditioned media from 18 lung adenocarcinoma cell lines collected at predetermined incubation times (Baseline, 1, 2, 4 and 6 h) as previously described [21,22].

For siKYNU experiments, media (RPMI + 10% FBS) were collected 24 h post conditioning. Conditioned media was centrifuged at  $2000 \times g$  for 10 min to remove residual debris and the supernatants were transferred and stored in  $-80^\circ\text{C}$  until use for metabolomics analysis.

### 2.6.2. Assessment of KP-Related Metabolites

Metabolomics analysis for KP-related metabolites was conducted on Waters Acquity™ 2D/UPLC system (Milford, MA, USA) with parallel column regeneration configuration using H-class quaternary solvent manager and I-class binary solvent manager coupled to a Xevo G2-XS quadrupole time-of-flight (qTOF) mass spectrometer. Mass spectrometry data was acquired on Xevo G2 XS qTOF in ‘sensitivity’ mode for positive electrospray ionization modes within a 50–1200 Da range.

### 2.6.3. Data Processing

Liquid chromatography mass spectrometry (LC-MS) and LC-tandem mass spectrometry (MSe) data were processed using Progenesis QI (Nonlinear, Waters, Milford, MA, USA) and values were reported as area units. Annotations for tryptophan, kynurenine, anthranilate and 3-hydroxyanthranilate were determined by matching accurate mass and retention times using authentic standards and by matching experimental tandem mass spectrometry data against the NIST MSMS or HMDB v3 theoretical fragmentations.

### 2.6.4. Data Normalization

To correct for injection order drift, each feature was normalized using data from repeat injections of quality control samples collected every 10 injections throughout the run sequence. Measurement data were smoothed by Locally Weighted Scatterplot Smoothing (LOESS) signal correction (QC-RLSC), as previously described [22].

### 2.7. TCGA and Oncomine Datasets

Gene expression data, mutational information, and clinical data from The Cancer Genome Atlas (TCGA) network project was download from cBioPortal [23] (<http://www.cbioportal.org/> (accessed on: 15 June 2021)). Gene expression data and associated clinical information for the Okayama Lung Study [24] was downloaded from the Oncomine database [25].

### 2.8. Immunohistochemistry

The immunohistochemistry used in this study comprised 124 surgically resected LUAD tumor specimens collected under an institutional review board protocol and archived as formalin-fixed, paraffin-embedded specimens in The University of Texas Specialized Program of Research Excellence thoracic tissue bank at The University of Texas MD Anderson Cancer Center. Patient characteristics for the analyzed cohort are provided in Table A2 in the Appendix B. Primary antibodies include KYNU (E-5, Santa Cruz, Santa Cruz, CA, USA, sc-390360, at 1:1000 dilution), PD-L1 (clone E1L3N, dilution 1:100; Cell Signaling Technology, Danvers, MA, USA), CD3 (T-cell lymphocytes; dilution 1:100; Dako), CD4 (helper T cell; Novocastra; clone 4B12, dilution 1:80; Leica Biosystems, Wetzlar, Germany), CD8 (cytotoxic T cell; clone CD8/144B, dilution 1:20; Thermo Fisher Scientific, Waltham, MA, USA), PD-1 (clone EPR4877-2, dilution 1:250; Abcam, Cambridge, UK), and FOXP3 (regulatory T cell; clone 206D, dilution 1:50; BioLegend, San Diego, CA, USA) [26].

Immunohistochemical expression of KYNU was evaluated in the cytoplasm of malignant cells using an H-score (% MCs with mild staining  $\times$  1 + % MCs with moderate staining  $\times$  2 + % MCs with strong staining  $\times$  3; range: 0–300). In this study, tumors which showed a >100 score for KYNU were considered positive for expression of the protein. The densities of cells expressing CD3, CD4, CD8, FOXP3, and PD-1 were evaluated using the Aperio nuclear algorithm and CD68 using Aperio cytoplasmic algorithm and counting the cells positive for them in five random square areas (1 mm<sup>2</sup> each) in both intratumoral and peritumoral compartments as described elsewhere [26]. Histologic assessment of each 1 mm<sup>2</sup> was performed to ensure that tumor tissue (at least 80% malignant cells and tumor stroma) was included in the selected intratumoral region, and only non-malignant cells were included in the peritumoral compartment. For this analysis, each area examined was overlapped with the sequential IHC slides to quantify each marker at the same location

of the tumor specimens. The average total number of cells positive for each marker in the 5 square areas was expressed in density per mm<sup>2</sup> [26]. Membranous PD-L1 expression in malignant epithelial cells and macrophages was analyzed using a cell membrane staining algorithm, and the staining intensity scored as 0 (no staining), 1+ (weak staining), 2+ (moderate staining), or 3+ (strong staining) and extension (percentage) of expression were determined. The PD-L1 H-scores for tumor tissues were determined by multiplying the staining intensity and reactivity extension values (range, 0–300).

### 2.9. Statistics

Statistical significance was determined using Kruskal–Wallis multiple comparison tests unless otherwise specified. Spearman correlation heatmaps, Cox proportional hazard models, and construction of Kaplan–Meier survival curves were carried out in R statistical software. Significance in survival distributions was determined by Mantel–Cox log-rank *t*-test. For survival analyses, we used the method described by Contal and O’Quigley [27] to derive an optimal change point for KYNU expression that yielded the largest difference between individuals in the two already defined groups (alive/dead) [22,28]. Variables included into the multivariable Cox proportional hazard models were based on the backward stepwise method (likelihood ratio).

Figures were generated in either GraphPad Prism v6 or R statistical software. We note that we chose to use quartiles in comparison of the bottom 25th and top 25th percentiles of KYNU mRNA expression with tumor immunophenotype as to highlight the effect between the most differential populations; Spearman correlation analyses based on the TCGA LUAD dataset using continuous variables for KYNU mRNA expression and gene signatures of tumor immune cell infiltrates.

## 3. Results

### 3.1. Analysis of the Protein Signature of KEAP1 Mutation in LUAD Cell Lines

We evaluated the proteomes of 47 LUAD (11 *KEAP1* mutant (mut) and 36 *KEAP1* wild-type (wt)) cell lines to identify protein signatures related to *KEAP1* mutation status (Table A1 in the Appendix B). Of the 3892 quantified proteins, 296 exhibited raw *p*-values < 0.05 (Figure 1A; Table S1 online). Differential analyses revealed kynureninase (KYNU), a downstream enzyme in the tryptophan-kynurenine pathway (KP), as one of the top overexpressed proteins in *KEAP1*mut LUAD cell lines (Figure 1A–C; Table S1 online). Other quantified enzymes in the KP were non-statistically significant between *KEAP1*mut and *KEAP1*wt LUAD cell lines, which includes the rate-limiting enzyme in *de novo* NAD<sup>+</sup> biosynthesis, quinolinate phosphoribosyltransferase (QPRT), that is downstream of KYNU (Table S1 online). Analysis of gene expression data from the Cancer Cell Line Encyclopedia (CCLE) for LUAD yielded concordant findings at the RNA level (Figure A2A,B in the Appendix B). The overall findings suggest that the *KEAP1*mut-associated increase in KYNU expression is independent from induction of the entire kynurenine pathway, as would be observed with increased *de novo* NAD<sup>+</sup> biosynthesis. Therefore, we focused our efforts toward the mechanism and biological consequence of KYNU upregulation in LUAD.

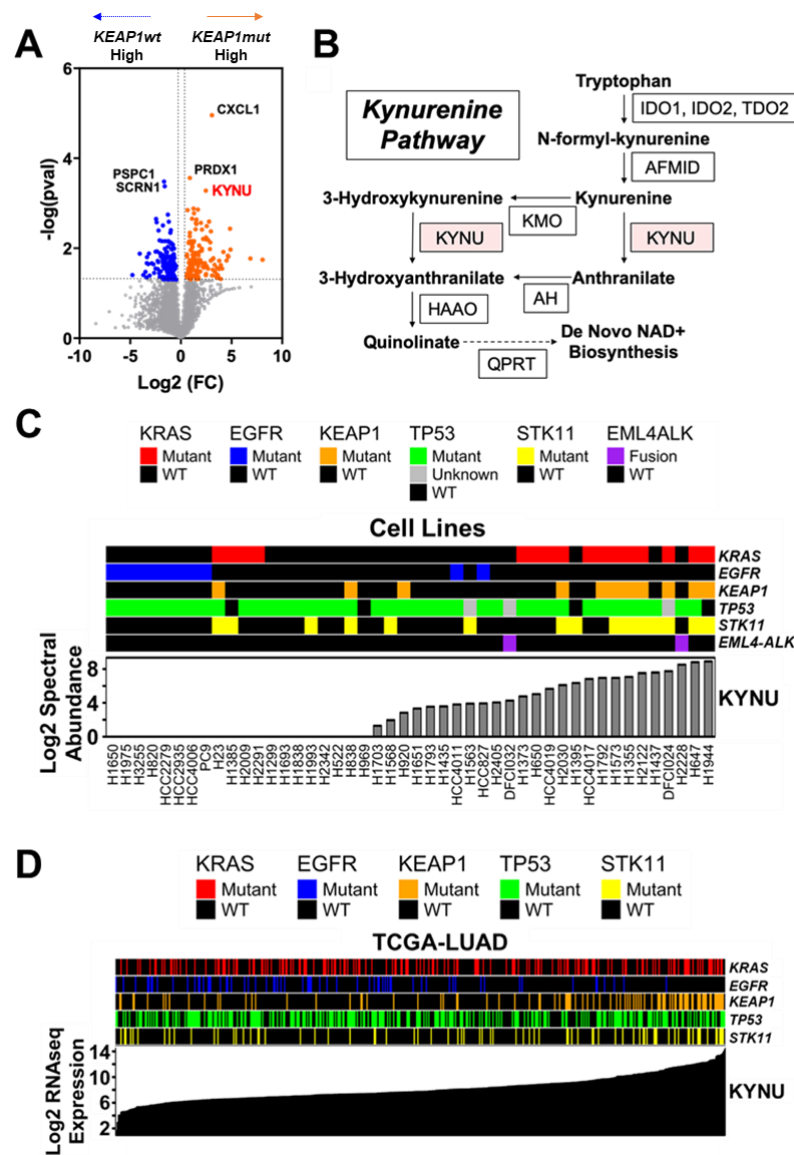


**Figure 1.** Lung Adenocarcinoma (LUAD) cell lines exhibit elevated KYNU expression. (A) Volcano plot illustrating differentially expressed proteins between *KEAP1*<sup>mt</sup> (n = 11) and *KEAP1*<sup>wt</sup> (n = 36) LUAD cell lines. Node color represent proteins that are statistically significantly (two-sided student *t*-test *p* < 0.05) increased (orange nodes) or decreased (blue nodes) in *KEAP1*<sup>mt</sup> LUAD cell lines. (B) Schematic of the kynurenine pathway (KP). (C) Association between whole cell lysate KYNU protein expression and presence of *KRAS*, *EGFR*, *KEAP1*, *TP53*, and *STK11* mutations and *EML4-ALK* fusions amongst 47 LUAD cell lines. KYNU expression is ranked from lowest to highest. (D) Association between KYNU mRNA expression and presence of *KRAS*, *EGFR*, *KEAP1*, *TP53*, and *STK11* mutations in TCGA-LUAD. KYNU mRNA expression is ranked from lowest to highest. Abbreviations: IDO—indoleamine 2,3-dioxygenase; TDO—tryptophan 2,3-dioxygenase; AFMID—kynurenine formamidase; KYNU—kynureninase; KMO—kynurenine 3-monooxygenase; AADAT—aminoadipate aminotransferase; HAAO—3-hydroxyanthranilate 3,4-dioxygenase; QPRT—quinolinic acid phosphoribosyltransferase.

### 3.2. KYNU Protein Expression Is Regulated by NRF2 Activation in Lung Adenocarcinoma

*KRAS*, *EGFR*, *TP53*, *KEAP1*, and *STK11* are the most prevalent mutations in LUAD and mutations in *STK11* frequently co-occur with *KEAP1* mutations [29,30]. Stratification of LUAD cell lines based on the occurrence of these mutations revealed a positive association between elevated KYNU protein expression and *KRAS*<sup>mut</sup> LUAD cell lines that harbor

mutations in *KEAP1* and *STK11* (Figure 1C; Figure A2C,D in the Appendix B). Analysis of The Cancer Genome Atlas (TCGA) LUAD gene expression dataset revealed a strong association between increased *KYNU* mRNA expression and occurrence of *KEAP1* mutations (Figure 1D; Figure A3A,B in the Appendix B).

To determine if NRF2 activation regulates *KYNU* expression, we performed siRNA-mediated knockdown of NRF2 in *KRAS/KEAP1/STK11* mutant LUAD cell lines H2030 and DFCI024, the results of which demonstrated reduced *KYNU* mRNA and protein expression (Figure 2A,B). No difference in *KYNU* protein expression was observed following siRNA-mediated knockdown of *STK11* (Figure A3C in the Appendix B).

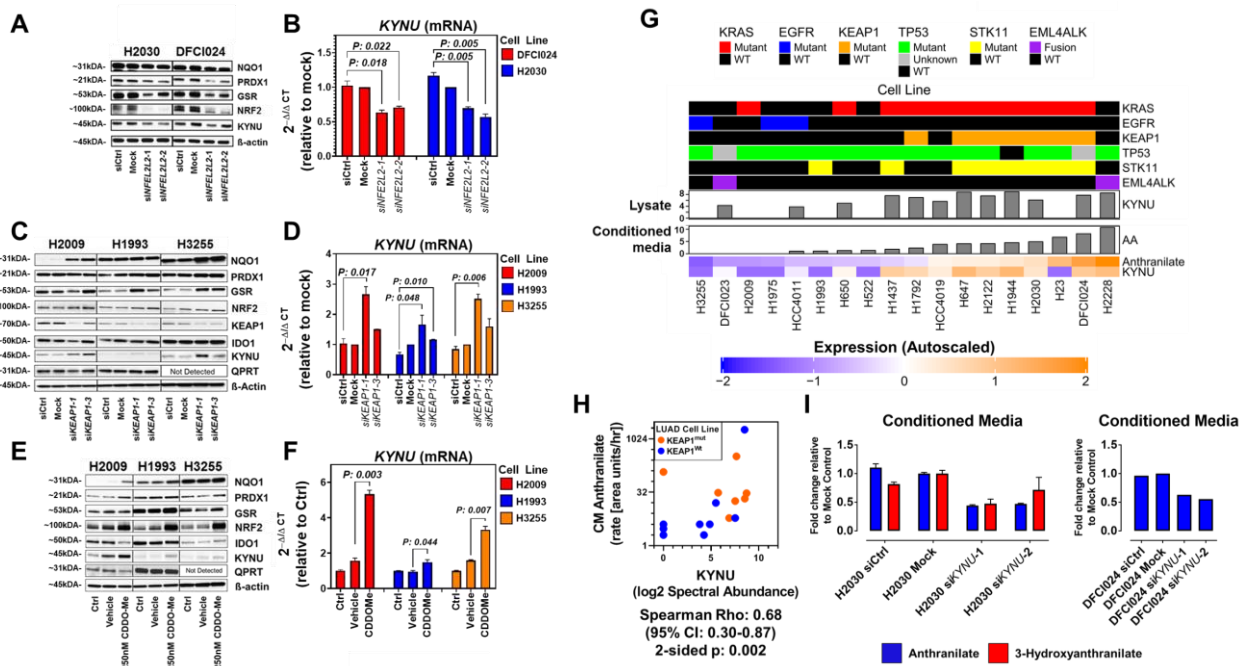


**Figure 2.** *KYNU* is regulated by NRF2 activation in lung adenocarcinomas and is functionally active. (A) Immunoblots for *KYNU*, NRF2 and NRF2-regulated enzymes peroxiredoxin 1 (PRDX1), glutathione reductase (GSR), and NAD(P)H quinone dehydrogenase 1 (NQO1) in *KEAP1/KRAS* mutant adenocarcinoma cell lines DFCI024 and H2030 following siRNA-mediated knockdown of the NRF2 transcribing gene *NFE2L2*. (B) mRNA expression ( $2^{-\Delta\Delta C_t}$ ) of *KYNU* following siRNA-mediated knockdown of *NFE2L2* in *KEAP1/KRAS* mutant adenocarcinoma cell lines DFCI024 and H2030. (C) Immunoblots for IDO1, *KYNU*, QPRT, *KEAP1*, NRF2, and NRF2-regulated enzymes PRDX1, GSR, and NQO1 following siRNA-mediated knockdown of *KEAP1* in H2009 (m*KRAS*), H1993 (*KRAS/EGFR* wild-type), and H3255 (m*EGFR*). (D) mRNA expression ( $2^{-\Delta\Delta C_t}$ ) of *KYNU* following siRNA-mediated knockdown of *KEAP1* in H2009, H1993, and H3255. (E) Immunoblots for IDO1, *KYNU*, QPRT, NRF2, and NRF2-regulated enzymes PRDX1, GSR, and NQO1 following 48-h treatment of H2009, H1993, and H3255 with NRF2-activator CDDOMe, vehicle (DMSO) or control media. (F) mRNA expression ( $2^{-C_t}$ ) of *KYNU* following 48-h treatment of H2009 (m*KRAS*), H1993 (*KRAS/EGFR* wild-type), and H3255 (m*EGFR*) with CDDOMe, vehicle or control media. CDDOMe: 2-Cyano-3,12-dioxo-oleana-1,9(11)-dien-28-oic acid methyl ester. (G) Heatmap illustrating the overall representation of whole lysate protein levels of *KYNU* and rates of anthranilate accumulation in conditioned media (CM) of 18 LUAD cell lines. Bar plots represent spectral abundance ( $\log_2$ ) of *KYNU* and rate ( $\log_2$  area units per hour per 500  $\mu\text{g}$  of protein) of anthranilate accumulation in conditioned media. Columns were ranked from by rate of anthranilate accumulation in CM from lowest to highest. (H) Scatter plot illustrating the association between whole lysate protein levels of *KYNU* and rates of anthranilate accumulation in conditioned media (CM) of 18 LUAD cell lines. Nodes represent whether the respective cell line was wild-type (wt; blue) or mutant (mut; orange) for *KEAP1*. (I) Conditioned media abundance of anthranilate and 3-hydroxyanthranilate following siRNA-mediated knockdown of *KYNU* in *KEAP1/KRAS* mutant LUAD cell lines H2030 and DFCI024.

Next, we activated NRF2 signaling in *KEAP1* wild-type/KYNU-low expressing LUAD cell lines H2009 (*KRAS*<sup>mut</sup>/*KEAP1*<sup>wt</sup>/*STK11*<sup>wt</sup>), H1993 (*KRAS*<sup>wt</sup>/*EGFR*<sup>wt</sup>/*KEAP1*<sup>wt</sup>/*STK11*<sup>mut</sup>) and H3255 (*EGFR*<sup>mut</sup>/*KEAP1*<sup>wt</sup>/*STK11*<sup>wt</sup>) via either siRNA-mediated knockdown of *KEAP1* or through chemical induction with the NRF2-activator CDDO-Me [31]. This led to increased protein and mRNA expression of KYNU (Figure 2C–F), implying that NRF2 could induce KYNU expression regardless of *KEAP1* mutation status.

To elucidate if KYNU was enzymatically functional, we performed metabolomic analyses using mass spectrometry on sequentially collected conditioned media (baseline, 30 min, 1 h, 2 h, 4 h and 6 h) from a subset of 18 LUAD cell lines. Analyses revealed a statistically significant positive correlation between the rate (area units/hour/100 µg of protein) of KYNU-derived anthranilate accumulation into conditioned media of LUAD cell lines with whole cell lysate KYNU protein concentration (Spearman  $\rho = 0.68$  (95% CI 0.30–0.87); 2-sided  $p$ -value = 0.002) (Figure 2G,H, Table A3 in the Appendix B). Knockdown of KYNU in *KRAS/KEAP1/STK11* mutant LUAD cell lines H2030 and DFCI024 decreased media anthranilate (Figure 2I), thereby confirming that KYNU is enzymatically functional in LUAD cell lines.

### 3.3. Association between Tumor KYNU Expression and Tumor Immunophenotype

KP pathway-related metabolites are known to elicit immunosuppressive functions, particularly through inhibition of T-cell activation and promotion of regulatory T cells (Treg) differentiation [32–35]. As we observed only an induction of KYNU and not the entire KP pathway, we evaluated whether KYNU alone could phenocopy this immunosuppression. We first analyzed TCGA-LUAD mRNA expression datasets (see Methods) [36]. Spearman correlation analyses revealed statistically significant positive correlations between KYNU mRNA expression and gene-based signatures of several immune cell subtypes, including cytotoxic CD8+ T cells ( $\rho = 0.28$  (95% CI 0.20–0.36); two-sided  $p < 0.0001$ ) and Tregs ( $\rho = 0.18$  (95% CI 0.10–0.27); two-sided  $p < 0.0001$ ), as well as immune checkpoint blockade-related genes *CD247* ( $\rho = 0.29$  (95% CI 0.20–0.37); two-sided  $p < 0.0001$ ), *PDCD1* ( $\rho = 0.24$  (95% CI 0.16–0.33); two-sided  $p < 0.0001$ ), and *CTLA4* ( $\rho = 0.21$  (95% CI 0.12–0.29); two-sided  $p < 0.0001$ ) (Figure 3A, Figure A4 in the Appendix B, Table S2 online). We performed additional sub-analyses on TCGA LUAD tumors that were wild-type for *KEAP1*. This revealed that KYNU mRNA expression retained statistically significant positive correlations with the signatures of cytotoxic CD8+ T cells ( $\rho = 0.38$  (95% CI 0.29–0.46); two-sided  $p < 0.0001$ ) and Tregs ( $\rho = 0.30$  (95% CI 0.21–0.39); two-sided  $p < 0.0001$ ), and expression of *CD247* (PD-L1) ( $\rho = 0.32$  (95% CI 0.23–0.41); two-sided  $p < 0.0001$ ), *PDCD1* (PD-1) ( $\rho = 0.30$  (95% CI 0.21–0.39); two-sided  $p < 0.0001$ ), and *CTLA4* ( $\rho = 0.30$  (95% CI 0.21–0.39); two-sided  $p < 0.0001$ ) (Figure 3A, Table S2 online). LUAD tumors with KYNU mRNA levels in the top 25th percentile exhibited statistically significantly elevated levels (two-sided Wilcoxon rank sum test  $p < 0.01$ ) signatures of CD8+ T cells and Tregs, and expression of *CD247* (PD-L1), *PDCD1* (PD-1), and *CTLA4*, as compared to those in the bottom 25th percentile (Figure 3B). Independent analysis of the Okayama [24] gene expression datasets yielded comparable findings (Figure A4 in the Appendix B).

Next, we performed immunohistochemistry for KYNU using a tissue microarray consisting of 124 LUAD tumors and compared KYNU protein levels (Figure 3C) with CD4+, CD8+, CD3+, and FOXP3+ immune-cell infiltrates, as well as PD-1 and PD-L1 staining positivity. Elevated KYNU protein expression was significantly positively associated with high numbers of CD8+ tumor infiltrating lymphocytes (TILs) (stratified by median, two-sided  $\chi^2$  test for Trend  $p = 0.007$ ), as well as PD-L1 cell positivity (stratified by median, two-sided  $\chi^2$  test for Trend  $p = 0.02$ ) (Figure 3D). No statistically significant association was observed between KYNU protein expression and staining positivity for CD3+, CD4+, FOXP3+, or PD-1. Collectively, these findings revealed that elevated KYNU expression is highly associated with an immunosuppressive tumor microenvironment.

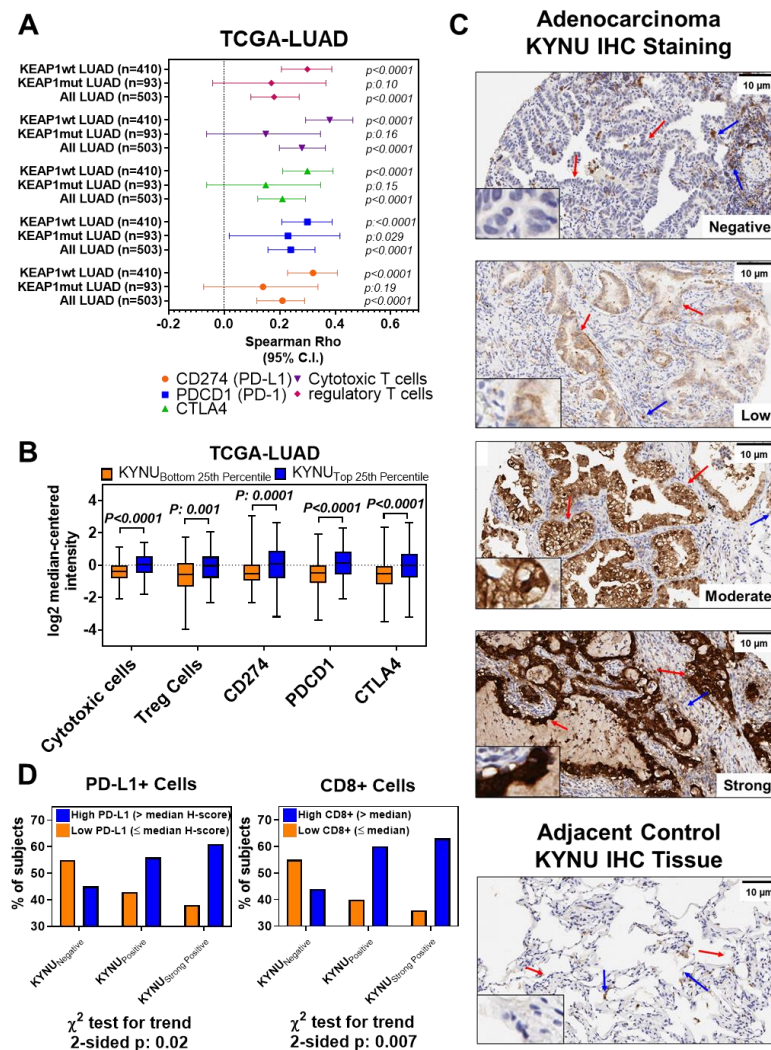


**Figure 3.** Association between KYNU and tumor immunophenotype. (A) Scatter plot illustrating Spearman correlations (95% CI) between continuous values of KYNU mRNA expression with gene-based signatures of cytotoxic T-cells, regulatory T cells, and immune checkpoint blocked related genes CD274 (PD-L1), PDCD1 (PD1), and CTLA4 in TCGA-LUAD tumors stratified by presence or absence of KEAP1 mutations. (B) Distribution of gene-based signatures reflective of cytotoxic T-cells, regulatory T cells, and immune checkpoint blockade-related genes CD274 (PD-L1), PDCD1 (PD1), and CTLA4 in TCGA-LUAD tumors stratified by KYNU mRNA expression into the bottom and top 25th percentiles. Statistical significance was determined by a two-sided Wilcoxon rank sum test. (C) Representative immunohistochemistry (IHC) staining of KYNU protein expression in adenocarcinoma TMA stratified by KYNU protein expression (negative, positive (50–150) and strong positivity (>150)), as well as adjacent control tissue. Red arrows indicate tumor tissue while blue arrows indicate inflammatory cell staining. Insets show a 5× enlargement. (D) Association between KYNU protein expression (negative, positive (50–150) and strong positivity (>150)) and PD-L1 staining positivity and CD8+ TILs (E) in LUAD TMAs. PD-L1 was stratified based on whether PD-L1 was >median of the H-Score (high) or ≤median of H-scores (low). CD8+ levels were stratified into either high (>median of positive cells per millimeter (mm)<sup>2</sup> tissue) or low (≤median of positive cells per mm<sup>2</sup> tissue). Statistical significance was determined by two-sided  $\chi^2$  test for trend.

### 3.4. Association between KYNU Tumor Expression and Overall Survival

We next evaluated the association between KYNU protein levels in a LUAD tissue microarray (TMA) and overall survival. In multivariate analyses, adjusted for stage, subjects with an optimal KYNU staining positivity cutoff of >120 exhibited statistically significantly worse overall survival compared to those subjects with KYNU staining positivity ≤ 120

(Hazard Ratio (HR) = 3.11 (95% CI 1.41–6.89), two-sided  $p = 0.005$ , Table 1, Kaplan–Meier survival curve in Figure 4A). A similar association between high *KYNU* expression and poorer overall survival was observed in LUAD gene expression datasets from Okayama lung study and TCGA (Figure 4B,C; Tables A4 and A5 in the Appendix B. Thus, elevated tumor *KYNU* expression is an independent prognostic marker of poor overall survival in LUAD.

**Table 1.** Cox proportional hazard models for *KYNU* protein expression and overall survival in lung adenocarcinoma TMA.

Variable	LUAD TMA					
	Univariable			Multivariable ‡		
	HR	95% CI	<i>p</i>	HR	95% CI	<i>p</i>
Sex						
Female		Reference			Reference	
Male	1.42	0.70–2.89	0.330		-	
Age †						
<65		Reference			Reference	
≥65	0.92	0.45–1.86	0.810		-	
Stage						
I		Reference			Reference	
II	3.69	1.43–9.53	0.007	4.12	1.59–10.69	0.004
III	7.74	2.98–20.10	<0.001	8.73	3.31–22.99	<0.001
IV	12.28	2.54–59.38	0.002	6.46	1.27–32.78	0.024
Smoking						
Never		Reference			Reference	
Former	1.11	0.36–3.40	0.860		-	
Current	1.23	0.40–3.73	0.720		-	
<i>KYNU</i> Staining †						
≤Cutoff		Reference			Reference	
>Cutoff	2.77	1.33–5.80	0.007	3.11	1.41–6.84	0.005

‡ Variables included into the equation after selection using a backward stepwise method (likelihood ratio). † cutoff was defined as *KYNU* positivity > or ≤120. † Stratified by median.

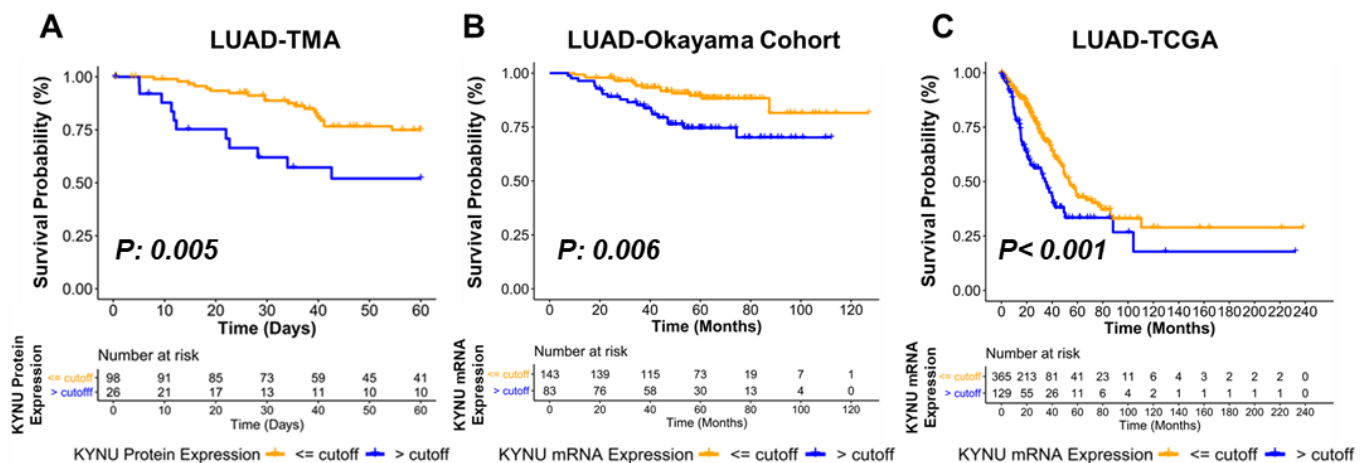


**Figure 4.** Association between *KYNU* and overall survival in LUAD. (A) Kaplan–Meier survival curves for five-year overall survival in adenocarcinoma TMAs based on a *KYNU* staining positivity cutoff of >120. Optimal cutoff value Figure 4. (B,C) Kaplan–Meier survival curves depicting overall survival in LUAD tumors stratified by an optimal cutoff value for *KYNU* mRNA Okayama and TCGA-LUAD gene expression datasets. Statistical significance was determined by two-sided log-rank Mantel–Cox test.

#### 4. Discussion

While both activation of the NRF2 pathway and aberrant tryptophan catabolism are strongly linked to an immunosuppressive milieu in tumors, these pathways have not been directly linked [34,37–40]. Here, we demonstrate a novel finding of NRF2-mediated KYNU upregulation in lung adenocarcinoma that is prognostic for poor overall survival. Mechanistic studies revealed that KYNU is activated by NRF2 signaling and that KYNU overexpression is associated with an immunosuppressive tumor microenvironment characterized by elevated tumor T-cell infiltration, including T regulatory TILs, and concordant increases in protein expression of immune checkpoint blockade-related PD1 and PD-L1 (Figure 5).

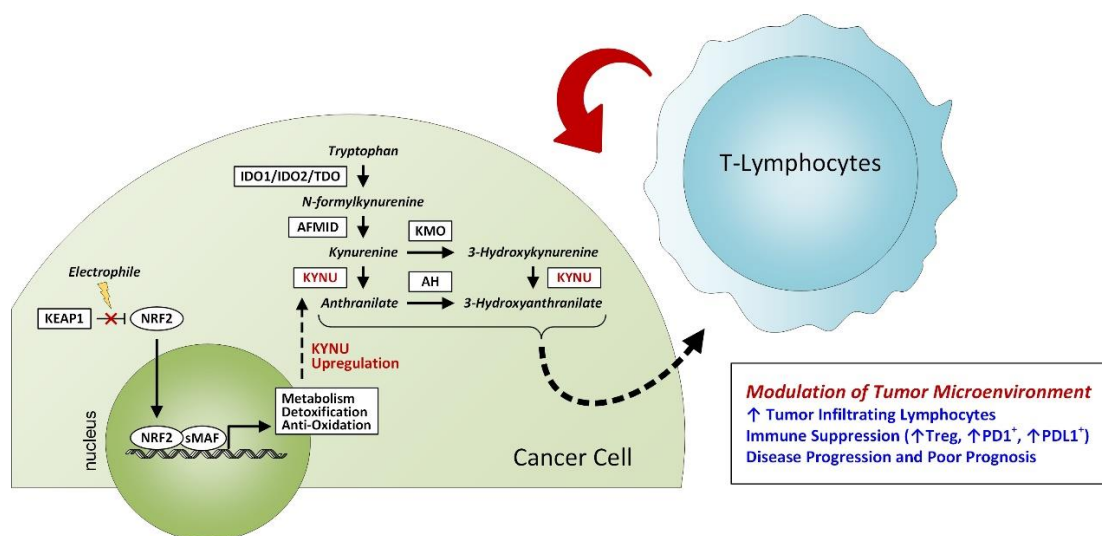


**Figure 5.** Proposed Schematic. NRF2 activation promotes KYNU upregulation in lung adenocarcinoma, resulting in an immunosuppressive tumor microenvironment characterized by elevated tumor T-cell infiltration, including T regulatory TILs, and concordant increases in protein expression of immune checkpoint blockade-related PD1 and PD-L1 and poor prognosis. Abbreviations: AFMID—arylformamidase; AH—anthranilate hydroxylase; IDO—indoleamine 2,3-dioxygenase; KEAP1—Kelch-like ECH-associated protein 1; KMO—kynurenine 3-monooxygenase; KYNU—kynureninase; NRF2—nuclear factor erythroid factor 2-related factor 2; PD1—programmed cell death protein-1; PDL1—programmed cell death ligand-1; sMAF—small musculoaponeurotic fibrosarcoma proteins; TDO—tryptophan 2,3-dioxygenase; Treg—regulatory T-cell.

A growing body of literature supports our observation that lung adenocarcinomas mutated for *KRAS* and with an activated NRF2 pathway have an altered tumor microenvironment that can, in part, be attributed to changes in tumor metabolism [16–18]. For instance, cancer cells harboring *KRAS* mutations have been shown to reprogram cancer cell metabolism towards an increase in uptake and catabolism of amino acids, such as glutamine and tryptophan, with pro-tumoral effects [41–43]. Reduced bioavailability of glutamine and tryptophan are reported to promote tumor immune suppression [35,44–47]. For example, depletion of tryptophan bioavailability in the tumor microenvironment triggers control non-derepressible 2 (GCN2)-mediated T-cell apoptosis [48] and attenuates T-cell proliferation, whereas increased accumulation of its downstream catabolite, kynurenine, promotes immune tolerance by inhibiting proliferation of T cells and natural killer cells and increasing proliferation of Tregs and myeloid derived suppressor cells [49,50]. These insights have thus led to several clinical trials specifically targeting tumor metabolism in *KRAS*/NRF2 tumors. For instance, the KEAPSAKE trial (Clinicaltrials.gov; NCT04265534) evaluated addition of a glutaminase inhibitor (telaglenastat) to standard-of-care immunotherapy and chemotherapy in advanced lung cancer. Similarly, intensive investigation into the kynurenine pathway has led to the development of several inhibitors including epacodostat

and indoximod, which target the rate-limiting enzymes in tryptophan metabolism IDO1, IDO2, and TDO [51]. Despite early success, a recent phase III double-blinded randomized trial of epacadostat/pembrolizumab versus pembrolizumab (ECHO-301) did not note additional benefit of epacadostat [52]. Plausible explanations for lack of additional efficacy can be attributed to insufficient inhibition of tryptophan catabolism or due to disparity in expression of IDO and TDO amongst different cancer types [20]. Additionally, other tryptophan catabolites in the kynurenine pathway, such as 3-hydroxyanthranilate, can exert immunosuppressive functions by directly inhibiting T-lymphocyte activation, promoting regulatory T cell (Treg) differentiation, and in mitigating non-antigen stimulated T-cell proliferation [39,53]. There remains interest in development of pleiotropic tryptophan pathway inhibitors or a combination of inhibitors that act on multiple enzymes within the kynurenine pathway. Our findings reported are therefore of direct relevance, by identifying a potential alternative target to attenuate immunosuppression. Further investigations exploring the targetability of KYNU as a ‘immuno-metabolic’ adjuvant in LUAD harboring *KEAP1* mutations are thus warranted.

Elevated levels of circulating tryptophan and kynurenine-pathway related metabolites have also been reported to be associated with an increase in risk of developing lung cancer [54,55] and poor overall survival [56,57]. A recent report demonstrated that elevated the plasma levels of 3HA, a metabolite derived via the catabolism of 3-hydroxykynurenine by KYNU, was associated with significantly worse progression free survival in NSCLC subjects [58]. Notably, in this study, the combination of high tumor PDL-1 expression with elevated plasma 3HA had the highest predictive accuracy of objective response to immune checkpoint inhibitors (ICI). Here, we report that KYNU is an independent prognostic indicator of poor overall survival in lung adenocarcinoma with increased CD8+ and T-regulatory lymphocyte infiltration into tumors. It has been demonstrated that in tumor-bearing immune competent mice, administration of pharmacologically optimized PEGylated kynureninase (PEG-KYNase) promoted anti-cancer effects via increases in tumor infiltration and expansion of CD8+ lymphocytes [20]. Discrepancies may be attributed to our finding that KYNU is regulated through NRF2 activation, which is a known predictor of poor patient survival [17,59,60]. Additionally, lung cancer commonly occurs in a background of a chronically inflamed lung, which could suppress T-cell function through immune checkpoint blockade or through exhaustion. This may reflect the dynamic nature of T-cell activation and suppression in the tumor microenvironment.

## 5. Conclusions

We have identified a distinct signature of perturbed tryptophan catabolism in subsets of lung adenocarcinomas with activated NRF2 characterized by elevated KYNU expression. Protein expression of KYNU serves as a promising prognostic marker for lung adenocarcinoma and may yield capacity to identify subjects who are likely to receive benefit from ICI therapy. Further exploration of KYNU in the context of lung adenocarcinoma and immunotherapy is warranted.

**Supplementary Materials:** The following supporting information can be downloaded at: <https://www.mdpi.com/article/10.3390/cancers14102543/s1>, Table S1. Differential proteins between *KEAP1*mut and *KEAP1*wt lung adenocarcinoma cell lines; Table S2. Spearman correlation analyses between KYNU mRNA expression and gene-based signatures of immune cell subtypes or immune check point blockade-related genes in TCGA-LUAD tumors stratified by the presence or absence of *KEAP1*/*STK11* mutations.

**Author Contributions:** Conceptualization, J.F.F. and E.J.O.; methodology, J.F.F., E.I., E.M., J.B.D. and H.K.; formal analysis, J.F.F., I.T., E.I., X.M., J.C., J.M., Q.P., M.C., S.P., H.K., J.C. and E.J.O.; investigation, J.F.F. and E.O.; resources, J.R.-C., C.B., I.W. and S.H.; data curation, J.F.F. and E.J.O.; writing—original draft preparation, J.F.F. and E.J.O.; writing—review and editing, I.T., E.I., X.M., J.B.D., E.M., J.C., J.M., Q.P., M.C., J.V.V., S.P., A.T., O.D., S.C.T., H.K., L.M.S.S., J.R.-C., C.B., I.W. and S.H.; visualization, J.F.F.; supervision, S.H. and E.O.; project administration, E.J.O.; funding acquisition, S.H. and E.J.O. All authors have read and agreed to the published version of the manuscript.

**Funding:** We thank the MD Anderson Moonshot project, the American Lung Association, and the Lyda Hill Foundation for supporting this research. We additionally acknowledge the MDACC histology core (NIH 2P30CA016672-38). All authors consent to publication of the work presented herein. This work was supported by a faculty fellowship from The University of Texas MD Anderson Cancer Center Duncan Family Institute for Cancer Prevention and Risk Assessment (JFF), the Lyda Hill Foundation, and the University of Texas MD Anderson Cancer Center Moonshot Program. EJO is supported by the American Lung Association Lung Cancer Discovery Award 619882.

**Institutional Review Board Statement:** Not applicable.

**Informed Consent Statement:** Not applicable.

**Data Availability Statement:** Relevant data supporting the findings of this study are available within the Article and Appendices, or are available from the authors upon reasonable request.

**Conflicts of Interest:** The authors declare no conflict of interest.

## Appendix A.

### *Appendix A.1. Cell Culture and Transfection*

Cancer cell lines were maintained in RPMI media plus 10% fetal bovine serum (FBS) unless otherwise stated. The identity of each cell line was confirmed by DNA fingerprinting via short tandem repeats at the time of mRNA and total protein lysate preparation using the PowerPlex 1.2 kit (Promega, Madison, WI, USA). Fingerprinting results were compared with reference fingerprints maintained by the primary source of the cell line.

Small interfering RNA (siRNA) transfection experiments were performed using the following siRNAs: siControl (Silencer Select Negative Control #1, Life Technologies, Carlsbad, CA, USA), siKYNU #1 and #2 (s17103 and s1704, Invitrogen, Waltham, MA, USA), siKEAP1 #1 and #2 (#00080908 and #00344034, Sigma Aldrich, St. Louis, MO, USA) and siNFE2L2 #1 and #2 (#00182393 and # 00341015, Sigma Alrich, St. Louis, MO, USA). Cells were transfected at a final concentration of 20 nM siRNA using Lipofectamine RNAiMAX (Life Technologies, Carlsbad, CA, USA), according to the manufacturer's instructions. Media was exchanged with fresh RPMI + 10% FBS 16-hours post-transfection. Cell lysates were collected 48 and 72 h post-transfection for RNA and protein isolation, respectively.

### *Appendix A.2. Western Blot Analysis*

Cells were washed three times with ice-cold 1X PBS (Gibco, Waltham, MA, USA), and then lysed with RIPA Buffer including Protease and Phosphatase Inhibitors (Roche Lifesciences, Basel, Switzerland). Protein concentration was measured using the Bradford reagent (BioRad, Hercules, CA, USA) and equal amounts of proteins (20 µg/lane) were resolved on SDS-PAGE (BioRad Hercules, CA, USA). Proteins were electro-transferred onto polyvinylidene-difluoride (PVDF) membrane. After blocking with 5% non-fat milk, blots were incubated with α-KYNU (Santa Cruz Biotechnology, Dallas, TX, USA, sc-390360), α-IDO (Abcam, ab55305), α-QPRT (Abcam, Cambridge, UK, ab171944), α-Nrf2 (Abcam, Cambridge, UK, ab62352), α-KEAP1 (ProteinTech, Rosemont, IL, USA, 10503-2-AP), α-NQO1 (Abcam, Cambridge, UK, ab34173), α-Peroxiredoxin-1 (Abcam, Cambridge, UK, ab41906) or α-glutathione reductase (Abcam, Cambridge, UK, ab128933) at 4 °C overnight on orbital shaker. β-Actin primary antibody (Sigma Aldrich, St. Louis, MO, USA) was used as a control for protein loading. HRP-conjugated secondary antibody was purchased from (Amersham Biosciences, Pittsburg, PA, USA). Protein bands were detected by the enhanced chemiluminescence method (BioRad) on HyBlot CL film.

### *Appendix A.3. RT-PCR Analysis*

RNA was extracted using RNeasy Extraction Kit (Qiagen, Germantown, ML, USA) according to manufacturer's protocol. Complementary DNA (cDNA) samples were prepared by combining 10 µL of RNA (100 ng) with 0.8 µL 100 mM dNTPs, 1 µL 10X MultiScribe reverse transcriptase, 1 µL of 10X reaction buffer, 2 µL random primers, 1 µL RNase in-

hibitor and 3.2  $\mu\text{L}$  of ultrapure water (all reagents purchased from Applied Biosciences). PCR cDNA preparation was performed using an Eppendorf Thermal Cycler. Cycling conditions were 25 °C/10 min, 37 °C/120 min, 85 °C/5 min, followed by returned to 4 °C. TaqMan PCR assay was performed with a 7500 Fast Real-Time PCR System using universal TaqMan PCR master mix (ThermoFisher, Waltham, MA, USA) and FAM<sup>TM</sup>-labeled probes for KYNU (Hs00187560\_m1) and KEAP1 (Hs00202227\_m1) and VIC<sup>TM</sup>-labeled probes for  $\beta\text{2M}$  (Hs\_00187842\_m1). PCR was carried out using a BioRad CFX Connect RT System. Cycling conditions were 50 °C/2 min, 95 °C/10 min followed by 40 cycles at 95 °C/15 s to 60 °C/1 min. Each sample was run in duplicate. Ct values for each gene were calculated and normalized to CT values for  $\beta\text{2M}$  ( $\Delta\text{CT}$ ). The  $\Delta\Delta\text{Ct}$  values were then calculated by normalization to the Ct values for control. Values are reported as  $2^{-\Delta\Delta\text{Ct}}$ .

#### Appendix A.4. Proteomic Analysis

Proteomic analyses were conducted on 47 lung cancer cell lines; each cell line was analyzed as a single replicate. To obtain whole cell extract,  $\sim 2 \times 10^7$  cells were lysed in 1 mL of PBS containing the detergent octyl-glucoside (OG) (1% *w/v*) and protease inhibitors (complete protease inhibitor cocktail, Roche Diagnostics), followed by sonication and centrifugation at  $20,000 \times g$  with collection of the supernatant. Protein extraction was performed in a solution containing 2% (*v/v*) Igepal CA-630 (Sigma-Aldrich, St. Louis, MO, USA) with cell disruption by sonication followed by centrifugation at  $20,000 \times g$ . Two milligrams of whole cell extracts were reduced in dithiothreitol (DTT) and alkylated with iodoacetamide before fractionation with reverse-phase high performance liquid chromatography (RP-HPLC). A total of 84 fractions were collected at a rate of 3 fractions/minute. The mobile phase A was: H<sub>2</sub>O: Acetonitrile (95:5, *v/v*) with 0.1% trifluoroacetic acid (TFA); mobile phase B was: Acetonitrile:H<sub>2</sub>O (95:5) with 0.1% TFA. The collected fractions from RP-HPLC were dried by lyophilization and subjected to in-solution digestion with trypsin (Trypsin Gold, Mass Spectrometry Grade, Promega). Trypsin powder was dissolved in the Digestion Buffer (100 mM amino bicarbonate, 2% Acetonitrile) to make 8 ng/ $\mu\text{L}$  of Trypsin solution. Then, 50  $\mu\text{L}$  of Trypsin solution was added to each of the dried fractions, capped and mixed thoroughly, followed by digestion for 5 h at 37 °C. The digestion was quenched by adding 10  $\mu\text{L}$  of quench solution (1%TFA in H<sub>2</sub>O). Based on the chromatogram profile, 84 fractions were grouped into 24-pool fractions for LC-MS/MS analysis by RPLC-MS/MS using a nanoflow LC system (Eksigent) coupled on-line with mass spectrometry (MS). Separations were performed using 75  $\mu\text{m}$  inner diameter  $\times$  360  $\mu\text{m}$  outer diameter  $\times$  25 cm long fused silica capillary column (New Objective) slurry packed in house with 5  $\mu\text{m}$ , 200 Å pore size C18 silica-bonded stationary phase (Magic C18 AQ, New Objective). Tryptic peptides corresponding  $\sim 2 \mu\text{g}$  amount of protein from each fraction was individually injected to on-line connected C18 trap column (Waters, 180  $\mu\text{m}$  ID  $\times$  20 mm), washed for 5 min with mobile phase A (2% acetonitrile, 0.1% formic acid) at a flow rate of 10  $\mu\text{L}/\text{min}$ . After the trap column desalting, peptides were eluted using a linear gradient up to 35% mobile phase B (0.1% formic acid in 95% acetonitrile) for 90 min, then increased to 95% B in 5 min, with a further additional wash with 95% B for 10 min at a constant flow rate of 300 nL/min. Eluted peptides were analyzed by LTQ Orbitrap mass spectrometer (Thermo Scientific, Waltham, MA, USA) in data dependent acquisition (DDA) mode. Each full MS scan (*m/z* 400–1800) was followed by 10 MS/MS scans (normalized collision energy of 35%) for the 10 most abundant precursor ions in a  $\sim 1.5$  s of duty cycle. Dynamic exclusion was enabled to minimize redundant selection of peptides previously selected for MS/MS analysis. Parameters for MS1 were 60,000 for resolution,  $1 \times 10^6$  for automatic gain control (AGC) target, and 150 ms for maximum injection time. MS/MS was done by collision-induced dissociation (CID) fragmentation with  $3 \times 10^4$  for AGC, 10 ms for maximum injection time, 35 for normalized collision energy (NCE), 2.0 *m/z* for isolation width, 0.25 for activation *q*-value, and 10 ms for activation time.

MS/MS spectra were searched against the Uniprot proteome database (Human and Bovine, January 2017) using the X!Tandem search engine through Trans-Proteomic Pipeline

(TPP 4.8) and processed with the peptide and protein prophet. For the modifications, one fixed modification of carbamidomethylation (57.04304 Da) or propionamide (71.037114) at cysteine and two variable modifications, oxidation at methionine (15.9949 Da) and SILAC 13C6 at lysine (6.0201 Da) were chosen. The mass error allowed was 20 ppm for parent monoisotopic and 0.5 Da for MS2 fragment monoisotopic ions. Trypsin was specified as protein cleavage site, with possibility of two missed cleavages allowed. A false protein discovery rate of approximately 5% was determined by searching the primary tandem MS data using the same criteria against a decoy database wherein the protein sequences are reversed. Any stable isotope unlabeled lysine containing peptides with bovine homology were discarded. The total number of spectral counts for each protein group was normalized to the total spectral counts of the sample and subsequently multiplied by a constant which was set as 50,000; scaled data was used for subsequent downstream analysis. Measurements were retained based on spectral counts > 5 for at least one cancer cell line type, resulting in a total of 3892 proteins that were kept for statistical analysis.

#### *Appendix A.5. Metabolomic Analysis*

##### *Appendix A.5.1. Exometabolome Experiments*

Each cell line was analyzed in biological triplicate or quadruplicate unless otherwise specified. Cells were grown in 1ml of RPMI 1640 + 10% FBS in 12-well dishes (Costar, Houston, TX, USA) to reach a 70% (50–80%) confluency, 24 h post initial seeding. On the day of the experiment, the cells were washed twice with 500  $\mu$ L serum free RPMI (Fisher Scientific) containing 5 mM glucose and 0.5 mM glutamine. Next, serum free RPMI (300  $\mu$ L) containing 5 mM glucose and 0.5 mM glutamine was added to each well and the cells were incubated. After predetermined incubation time (1, 2, 4 and 6 h), 250  $\mu$ L of the conditioned media was collected. For baseline (T0), 250  $\mu$ L of media was collected directly after the addition of 300  $\mu$ L. Blank samples containing media only were included and collected at T0 and T6. The 6 h samples were used to count cell numbers for data normalization. Once all the media samples were collected, the tubes were centrifuged at  $2000\times g$  for 10 min to remove residual debris and the supernatants transferred to 1.5 mL tubes (Eppendorf, Hamburg, Germany), and stored in  $-80\text{ }^{\circ}\text{C}$  until use for metabolomics analysis.

##### *Appendix A.5.2. Mass Spectrometry Data Acquisition*

Frozen media samples were thawed on ice and 30  $\mu$ L transferred to a 96-well microplate (Eppendorf) containing 30  $\mu$ L of 100 mM ammonium formate, pH 3.0. The microplates were heat sealed, vortexed for 5min at 750 rpm, and centrifuged at  $2000\times g$  for 10 min at room temperature. For hydrophilic interaction liquid chromatography (HILIC) analysis, 25  $\mu$ L of sample was transferred to a new 96-well microplate containing 75  $\mu$ L acetonitrile, whereas samples for C18 analysis were transferred to a new 96-well microplate containing 75  $\mu$ L water (GenPure ultrapure water system, Thermofisher, Waltham, MA, USA). Each sample solution was transferred to a 384-well microplate (Eppendorf, Hamburg, Germany) for LCMS analysis. Samples were randomized during LCMS analysis and a matrix-matched reference quality controls and batch-specific pooled quality controls were included.

Untargeted metabolomics analysis was conducted on Waters Acquity™ 2D/UPLC system with parallel column regeneration configuration using H-class quaternary solvent manager and I-class binary solvent manager coupled to a Xevo G2-XS quadrupole time-of-flight (qTOF) mass spectrometer. Chromatographic separation was performed using HILIC (Acquity™ UPLC BEH amide, 100 Å, 1.7  $\mu$ m 2.1  $\times$  100 mm, Waters Corporation, Milford, CT, USA) and C18 (Acquity™ UPLC HSS T3, 100 Å, 1.8  $\mu$ m, 2.1  $\times$  100 mm, Water Corporation, Milford, CT, USA) columns at 45  $^{\circ}\text{C}$ .

Quaternary solvent system mobile phases were (A) 0.1% formic acid in water, (B) 0.1% formic acid in acetonitrile and (D) 100 mM ammonium formate, pH 3. Samples were eluted using the following gradient profile: for the HILIC analysis, a starting gradient of 95% B and 5% D was increased linearly to 70% A, 25% B and 5% D over a 5 min period at 0.4 mL/min

flow rate, followed by 1 min isocratic gradient at 100% A at 0.4 mL/min flow rate. For the reverse phase C18 analysis, the chromatography gradient was as follows: starting conditions, 100% A, with linear gradient to final conditions of 5% A, 95% B followed by isocratic gradient at 95% B, 5% D for 1 min.

Binary solvent manager was used for column regeneration and equilibration, with the following mobile phases: (A1) 100 mM ammonium formate, pH 3, (A2) 0.1% formic in 2-propanol, and (B1) 0.1% formic acid in acetonitrile.

Mass spectrometry data was acquired on Xevo G2 XS qTOF in 'sensitivity' mode for positive electrospray ionization mode within a 50–1200 Da range. For the electrospray acquisition, the capillary voltage was set at 1.5 kV (positive), sample cone voltage 30 V, source temperature at 120 °C, cone gas flow 50 L/h, desolvation temperature 400 °C and desolvation gas flow rate of 800 L/h with scan time of 0.5 s in continuum mode. Leucine enkephalin [556.2771 Da (positive)] was used for lockmass correction, and scans were performed every 0.5 min. The samples were injected randomly at 3 µL volume.

#### Appendix A.5.3. Data Processing

LC-MS and LC-MSe data were processed using Progenesis QI (Nonlinear, Waters) and values were reported as area units. Annotations for tryptophan, kynurenine, anthranilate and 3-hydroxyanthranilate were determined by matching accurate mass and retention times using customized libraries created from authentic standards and/or by matching experimental tandem mass spectrometry data against the NIST MSMS or HMDB v3 theoretical fragmentations.

#### Appendix A.5.4. Data Normalization

To correct for injection order drift, each feature was normalized using data from repeat injections of quality control samples collected every 10 injections throughout the run sequence. Measurement data were smoothed by Locally Weighted Scatterplot Smoothing (LOESS) signal correction (QC-RLSC) as previously described [28]. Feature values between quality control samples were interpolated by a cubic spline. Metabolite values were rescaled by using the overall median of the historical quality control peak areas across all samples. Only detected features exhibiting a relative standard deviation (RSD) less than 30% for either the historical or pooled quality controls samples were considered for further statistical analysis. Calculated rates were adjusted to total cell protein.

#### Appendix A.6. Immunohistochemical Analysis

The immunohistochemistry used in this study comprised 124 surgically resected LUAD tumor specimens collected under an institutional review board protocol and archived as formalin-fixed, paraffin-embedded specimens in The University of Texas Specialized Program of Research Excellence thoracic tissue bank at The University of Texas MD Anderson Cancer Center. Patient characteristics for the analyzed cohort are provided in Table A1 in the Appendix B. Tumor staging was performed using the staging system from the 7th American Joint Committee on Cancer. For adenocarcinoma, predominant histologic pattern (solid, lepidic, acinar, papillary, and micropapillary) was determined according to the 2015 World Health Organization classification. TMA sections were stained in a Leica Bond Max autostainer (Leica Biosystems Nussloch GmbH, Nußloch, Germany). Four micrometer-thick tissue sections (4 µm) were deparaffinized and rehydrated following the Leica Bond protocol. Antigen retrieval was performed for 20 min with Bond Solution # 1 (Leica Biosystems, equivalent Citrate Buffer, pH6, AR9961). The slides were then incubated with the primary antibody for KYNU (E-5, Santa Cruz, sc-390360, at 1:1000 dilution), PD-L1 (clone E1L3N, dilution 1:100; Cell Signaling Technology), CD3 (T-cell lymphocytes; dilution 1:100; Dako), CD4 (helper T cell; Novocastra; clone 4B12, dilution 1:80; Leica Biosystems), CD8 (cytotoxic T cell; clone CD8/144B, dilution 1:20; Thermo Fisher Scientific), PD-1 (clone EPR4877-2, dilution 1:250; Abcam), and FOXP3 (regulatory T cell; clone 206D, dilution 1:50; BioLegend) [26] As an external positive control for KYNU staining, we used non-neoplastic

liver tissue stained with KYNU antibody, but we substituted the KYNU antibody with diluent for negative control (Figure A5 in the Appendix B).

The IHC staining was revealed using the Bond Polymer Refine detection kit (Leica Biosystems DS9800), including 3/3'-diaminobenzidine as chromogen and hematoxylin as counterstaining. All slides were cover-slipped, and then scanned in an Aperio AT2 scanner. Three tissue microarray cores from each patient were evaluated, and the percentages of staining were averaged to provide the final scoring. For the immunostaining scoring, two board-certified surgical pathologists participated in the analysis of this tissue microarray. Before the tissue microarray scoring, the two pathologists evaluated together, at a double-headed microscope, the immunostaining pattern for KYNU in control slides and in the tissue microarray slides to agree on the criteria for intensity and percentage of staining. After scoring, the two pathologists met again to review the tissue microarray scoring together in the double-headed microscope and resolve any question or discrepancy in the evaluation. Immunohistochemical expression of KYNU was evaluated in the cytoplasm of malignant cells using an H-score (% MCs with mild staining  $\times 1$  + % MCs with moderate staining  $\times 2$  + % MCs with strong staining  $\times 3$ ; range: 0–300). In this study, tumors, which showed more than 100 score for KYNU were considered positive for expression of the protein. The densities of cells expressing CD3, CD4, CD8, FOXP3 and PD-1 were evaluated using the Aperio nuclear algorithm and CD68 using Aperio cytoplasmic algorithm and counting the cells positive for them in five random square areas (1 mm<sup>2</sup> each) in both intratumoral and peritumoral compartments, as described elsewhere [26]. Histologic assessment of each 1 mm<sup>2</sup> was performed to ensure that tumor tissue (at least 80% malignant cells and tumor stroma) was included in the selected intratumoral region, and only non-malignant cells were included in the peritumoral compartment. For this analysis, each area examined was overlapped with the sequential IHC slides to quantify each marker at the same location of the tumor specimens. The average total number of cells positive for each marker in the five square areas was expressed in density per mm<sup>2</sup> [26]. Membranous PD-L1 expression in malignant epithelial cells and macrophages was analyzed using a cell membrane staining algorithm, and the staining intensity scored as 0 (no staining), 1+ (weak staining), 2+ (moderate staining), or 3+ (strong staining), and extension (percentage) of expression was determined. The PD-L1 H-scores for tumor tissues were determined by multiplying the staining intensity and reactivity extension values (range, 0–300).

#### Appendix A.7. Statistical Analysis

For survival analyses, we used the method described by Contal and O'Quigley [27] to derive an optimal cut-off point for KYNU protein staining intensity that yielded the largest difference between individuals in the two already defined groups (alive/dead) [22,28]. Using log rank statistic based on the groups defined by cutoff yielded:

$$S_k = \sum_{i=1}^D [d_i^+ - d_i \frac{r_i^+}{r_i}]$$

where  $D$  is the total number of distinct death times,  $d_i$  is the total number of deaths at each event time ( $t_i$ ),  $d_i^+$  is the total number of death when KYNU staining value is bigger than the cut-off point.  $r_i$  and  $r_i^+$  are also defined as the total number at risk for all KYNU staining values and KYNU staining value larger than cut-off point, respectively. We calculated  $S_k$  for all possible cut points in the KYNU staining column and the estimated cut point as the value that yields the maximum  $S_k$ . Our analysis yielded a resultant KYNU protein staining positivity cutoff value of 120.

## Appendix B.

Table A1. Profiled lung adenocarcinoma cell lines.

Cell Line	KEAP1	LKB1 (STK11)	TP53	EGFR	KRAS	EML4ALK
H23	Mutant	Mutant	Mutant	WT	Mutant	WT
H838	Mutant	Mutant	Mutant	WT	WT	WT
H2030	Mutant	Mutant	Mutant	WT	Mutant	WT
H1573	Mutant	Mutant	Mutant	WT	Mutant	WT
H1792	Mutant	WT	Mutant	WT	Mutant	WT
H1355	Mutant	Mutant	Mutant	WT	Mutant	WT
H2122	Mutant	Mutant	Mutant	WT	Mutant	WT
H647	Mutant	Mutant	Mutant	WT	Mutant	WT
H920	Mutant	WT	Mutant	WT	WT	WT
DFCI024	Mutant	Mutant	Unknown	WT	Mutant	WT
H1944	Mutant	Mutant	WT	WT	Mutant	WT
PC9	WT	WT	Mutant	Mutant	WT	WT
H1299	WT	WT	Mutant	WT	WT	WT
H1975	WT	WT	Mutant	Mutant	WT	WT
H2009	WT	WT	Mutant	WT	Mutant	WT
H1437	WT	Mutant	Mutant	WT	WT	WT
H1650	WT	WT	Mutant	Mutant	WT	WT
H1568	WT	Mutant	Mutant	WT	WT	WT
H650	WT	WT	Mutant	WT	Mutant	WT
H3255	WT	WT	Mutant	Mutant	WT	WT
HCC4019	WT	WT	Mutant	WT	Mutant	WT
H1373	WT	WT	Mutant	WT	Mutant	WT
HCC827	WT	WT	Mutant	Mutant	WT	WT
H1693	WT	WT	Mutant	WT	WT	WT
H1993	WT	Mutant	Mutant	WT	WT	WT
HCC4011	WT	WT	Mutant	Mutant	WT	WT
HCC2279	WT	WT	Mutant	Mutant	WT	WT
H2228	WT	WT	Mutant	WT	WT	Fusion
HCC4006	WT	WT	Mutant	Mutant	WT	WT
H2405	WT	WT	Mutant	WT	WT	WT
H522	WT	WT	Mutant	WT	WT	WT
H820	WT	WT	Mutant	Mutant	WT	WT
H2291	WT	WT	Mutant	WT	Mutant	WT
HCC4017	WT	WT	Mutant	WT	Mutant	WT
HCC2935	WT	WT	Mutant	Mutant	WT	WT
H1703	WT	WT	Mutant	WT	WT	WT
H3255	WT	WT	Mutant	Mutant	WT	WT
H1793	WT	WT	Mutant	WT	WT	WT
H1651	WT	WT	Mutant	WT	WT	WT
H1435	WT	WT	Mutant	WT	WT	WT
H2342	WT	WT	Mutant	WT	WT	WT
H1838	WT	WT	Mutant	WT	WT	WT
DFCI032	WT	WT	Unknown	WT	WT	Fusion
H1563	WT	Mutant	Unknown	WT	WT	WT
H1395	WT	Mutant	WT	WT	WT	WT
H969	WT	WT	WT	WT	WT	WT
H1385	WT	Mutant	WT	WT	Mutant	WT

**Table A2.** Patient characteristics for lung adenocarcinoma TMA.

Characteristic	KYNU Immunostaining			<i>p</i>
	Total	Positive, n (%)	Negative, n (%)	
Total	124	31 (25.0)	93 (75.0)	
Sex				
Male	67	19	48	
Female	57	12	45	
Age				
>65 years	58	14	44	
≤65 years	66	17	49	
Smoking Status				
Current	44	17	37	
Former	44	13	41	
Never	16	1	15	
Stage				
I	69	16	53	0.2935
II	29	5	24	
III	24	9	15	
IV	2	1	1	
Mutations				
<i>KRAS</i>	24	11	22	0.1722
<i>EGFR</i>	11	1	13	
<i>KRAS</i> and <i>EGFR</i> wildtype	48	16	45	

**Table A3.** Secretion or uptake rates for anthranilate and 3-hydroxyanthranilate for 18 lung adenocarcinoma cell lines.

Cell Line	<i>KEAP1</i> Status	Whole Lysate KYNU Protein Expression ‡	Anthranilate †‡	3-Hydroxyanthranilate †‡
H647	Mutant	368	21 ± 9	-
DFCI024	Mutant	200	326 ± 87	-
H1944	Mutant	417	30 ± 15	-
H23	Mutant	0	119 ± 27	-
H1792	Mutant	118	6 ± 2	-
H2030	Mutant	52	31 ± 4	149 ± 6
H2122	Mutant	182	18 ± 3	3 ± 2
H1437	WT	183	6 ± 5	-
H2009	WT	0	2 ± 2	-
H1993	WT	0	4 ± 3	-
H3255	WT	0	0 ± 2	-
H2228	WT	362	1836 ± 279	-
DFCI023	WT	18	2 ± 3	-
H522	WT	0	4 ± 3	-
H650	WT	28	4 ± 3	-
HCC4011	WT	13	4 ± 3	-
H1975	WT	0	3 ± 4	-
HCC4019	WT	44	16 ± 3	-

† Values adjusted to total cell volume; ‡ Spectral Abundance based on proteomic analyses; ‡ Rate (Area Units/hr) +/- 95% CI of respective metabolite accumulation or depletion in conditioned media.

**Table A4.** Univariate and multivariate Cox proportional hazard models for KYNU mRNA expression in the TCGA-LUAD gene expression dataset.

Variable	Tcga LUAD Dataset					
	Univariable			Multivariable <sup>‡</sup>		
	Hazard Ratio	95% CI	Two-Sided <i>p</i>	Hazard Ratio	95% CI	Two-Sided <i>p</i>
<b>Sex</b>						
Female		Reference			Reference	
Male	1.05	0.78–1.42	0.73		-	
<b>Age</b>						
<66		Reference			Reference	
≥66	1.28	0.95–1.73	0.10	1.25	0.92–1.69	0.16
<b>Stage</b>						
I		Reference			Reference	
II	2.29	1.58–3.30	<0.0001	2.04	1.40–2.97	0.0002
III	3.56	2.43–5.23	<0.0001	3.12	2.11–4.59	<0.0001
IV	3.61	2.05–6.36	<0.0001	3.05	1.71–5.42	0.0001
<b>KYNU mRNA expression Cutoff<sup>‡</sup></b>						
≤cutoff		Reference			Reference	
>cutoff	1.83	1.35–2.50	0.0001	1.53	1.11–2.12	0.01

<sup>‡</sup> Optimal cut-off value (see methods); <sup>‡</sup> Variables included into the equation after selection using a backward stepwise method (likelihood ratio).

**Table A5.** Univariate and multivariate Cox proportional hazard models for KYNU mRNA expression in the Okayama lung adenocarcinoma gene expression dataset.

Variable	Okayama LUAD Dataset					
	Univariable			Multivariable <sup>‡</sup>		
	Hazard Ratio	95% CI	Two-Sided <i>p</i>	Hazard Ratio	95% CI	Two-Sided <i>p</i>
<b>Sex</b>						
Female		Reference			Reference	
Male	1.52	0.78–2.96	0.22		-	
<b>Age</b>						
<61		Reference			Reference	
≥61	1.43	0.73–2.78	0.29	1.68	0.86–3.29	0.13
<b>Stage</b>						
I		Reference			Reference	
II	4.23	2.17–8.24	<0.001	4.09	2.08–8.02	<0.001
<b>Smoking</b>						
Never		Reference			Reference	
Former/Current	1.64	0.84–3.20	0.15		-	
<b>KYNU mRNA expression Cutoff<sup>‡</sup></b>						
≤cutoff		Reference			Reference	
>cutoff	2.50	1.28–4.89	0.007	2.20	1.12–4.33	0.022

<sup>‡</sup> Optimal cut-off value (see methods); <sup>‡</sup> Variables included into the equation after selection using a backward stepwise method (likelihood ratio).

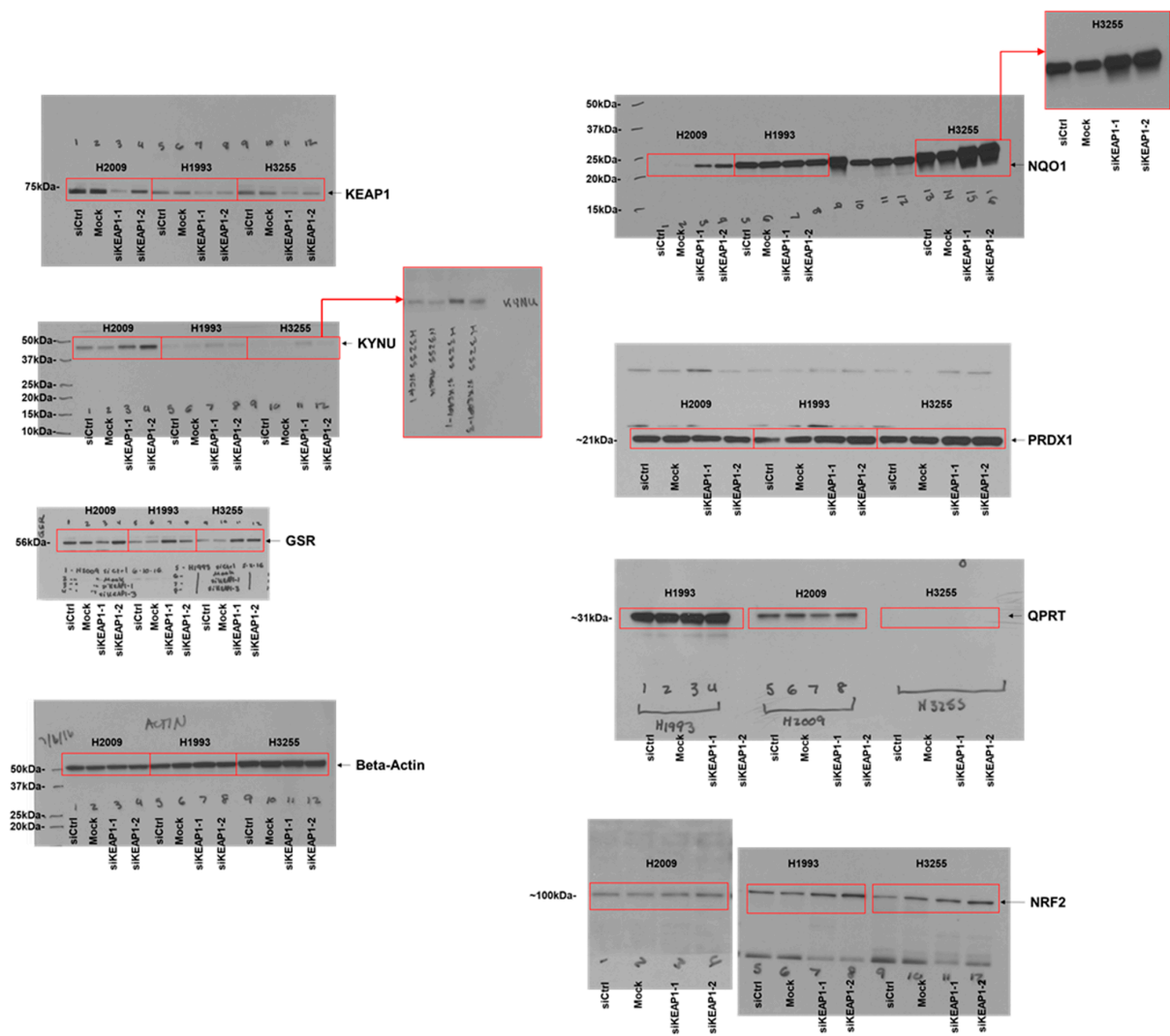


Figure A1. Cont.

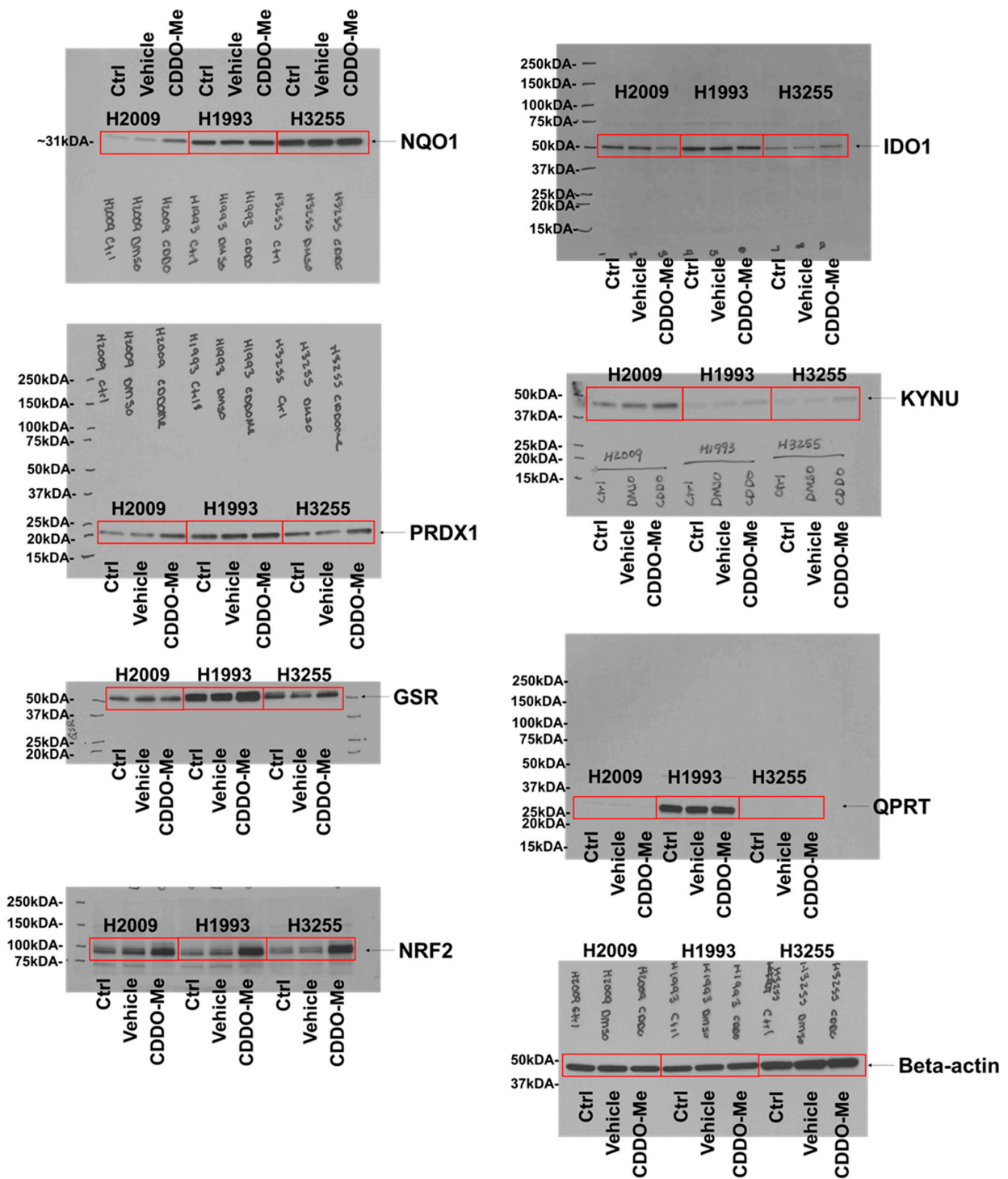


Figure A1. Cont.

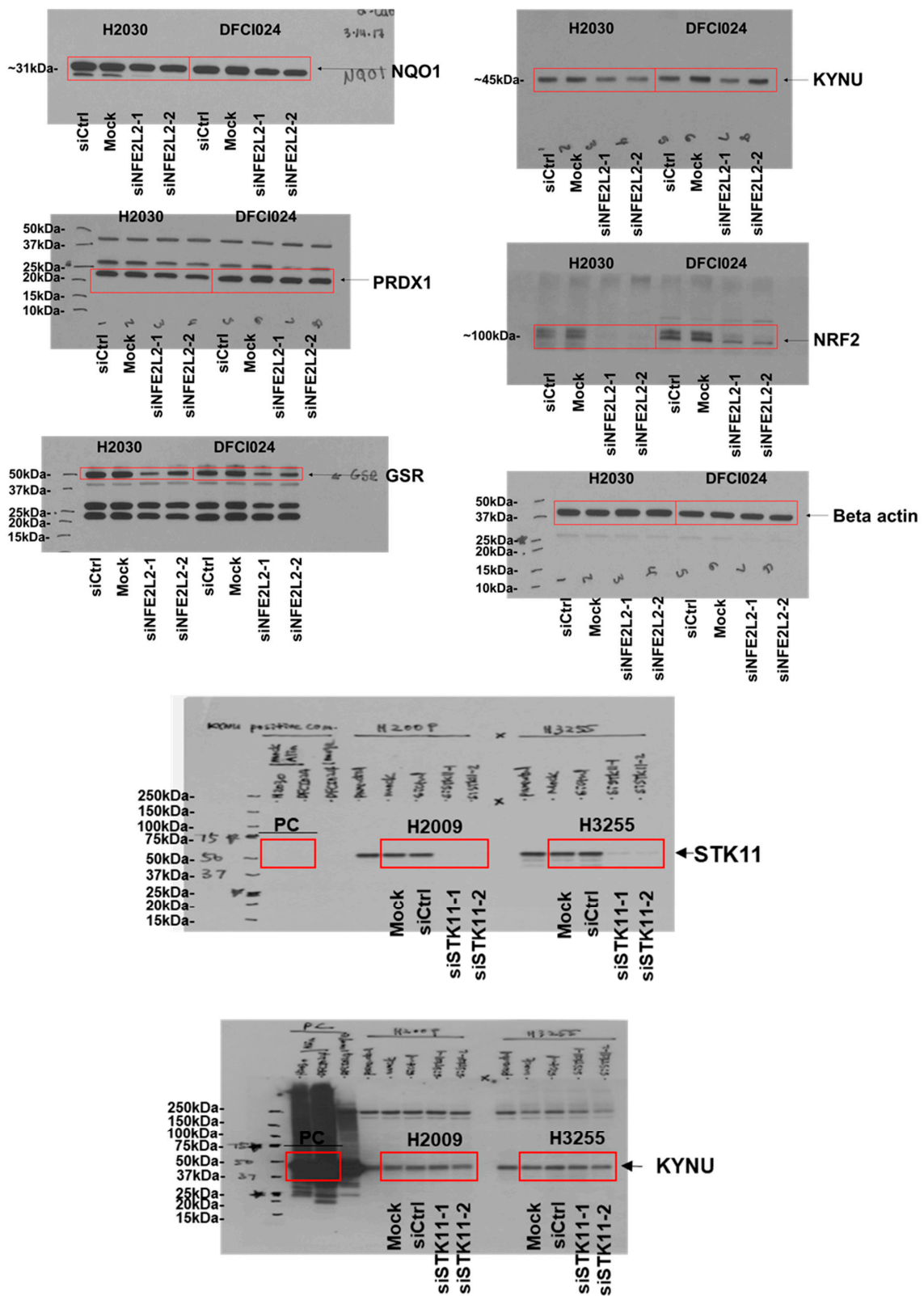


Figure A1. Cont.

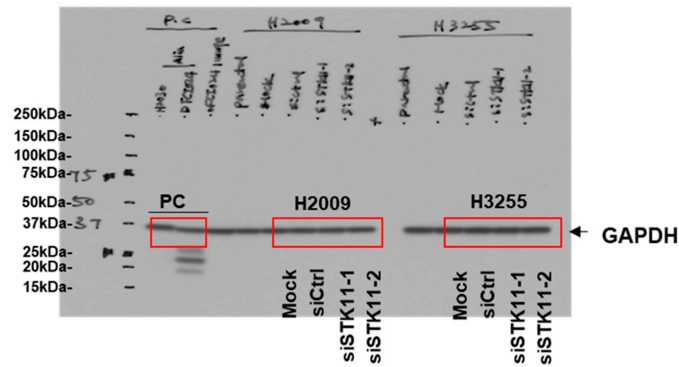
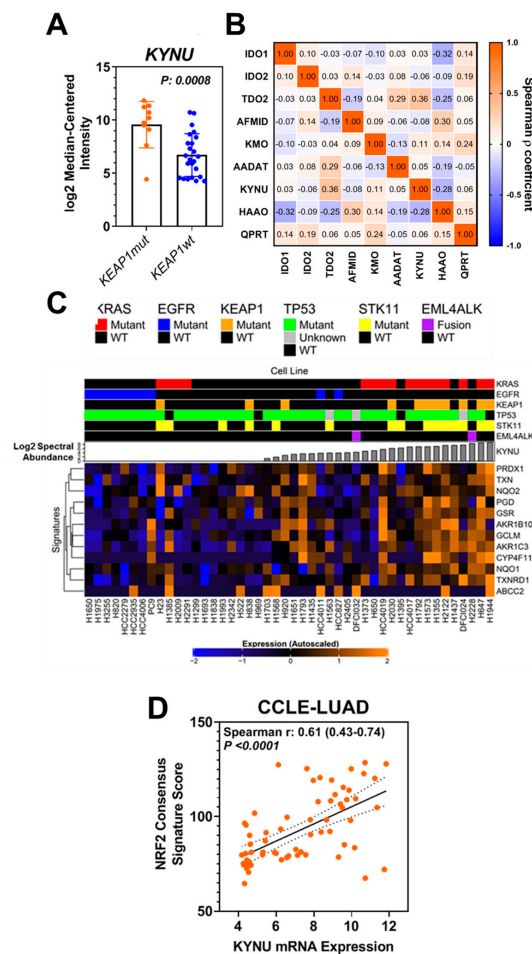
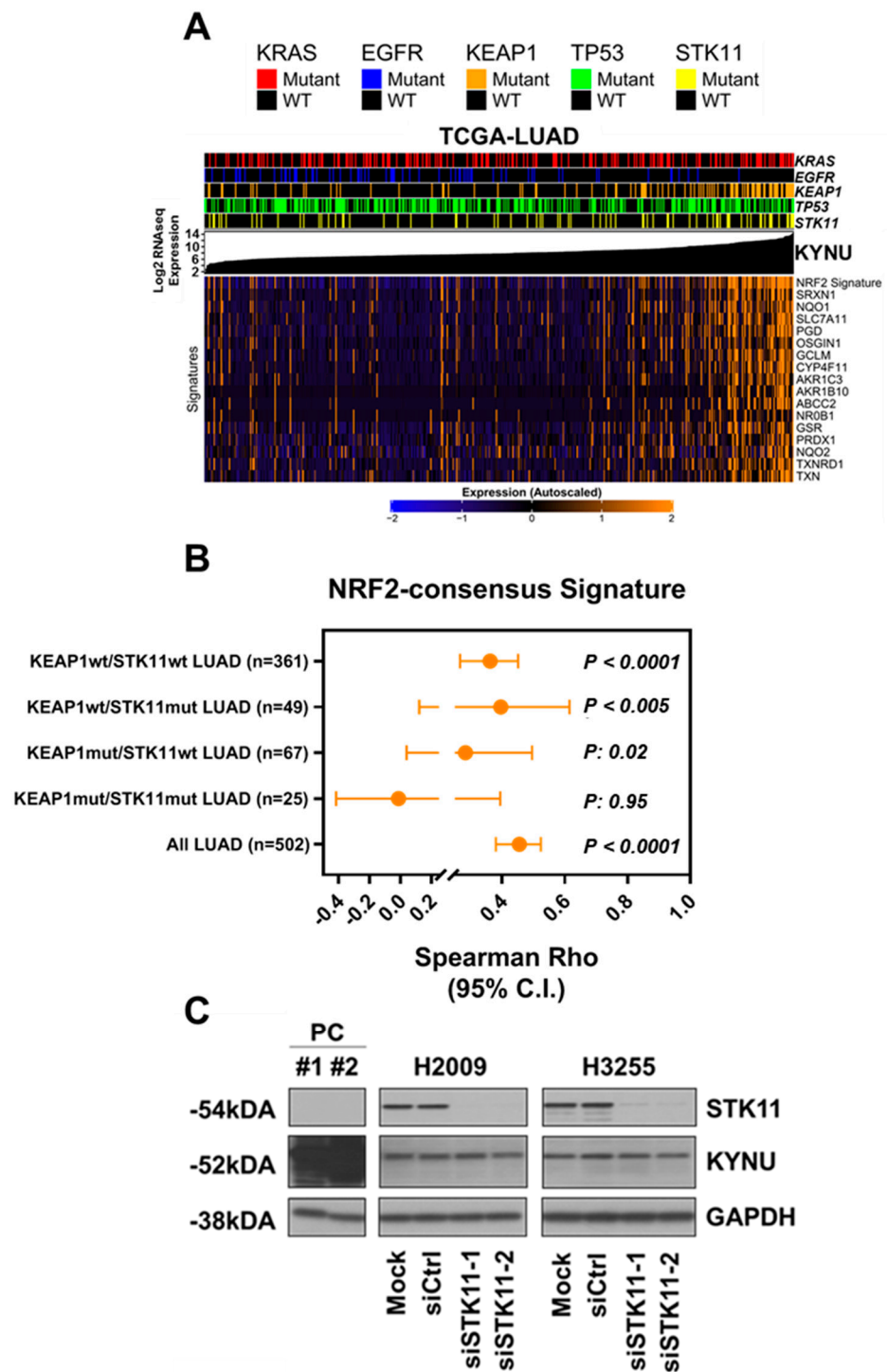


Figure A1. Uncut immunoblots.



**Figure A2.** Association between KYNU and tryptophan-kynurenine pathway metabolites and *KEAP1* mutation status in LUAD cell lines. **(A)** mRNA expression of KYNU in LUAD cell lines stratified by *KEAP1* mutational status. Gene expression was derived from the Cancer Cell Line Encyclopedia (CCLE) database and overlapped with cell lines for which proteomic data was available. **(B)** Heatmap depicting Spearman correlation coefficients between CCLE-derived mRNA expression of KYNU and associated tryptophan-kynurenine pathway-related enzymes among LUAD cell lines. **(C)** Heatmap representing protein expression of NRF2-downstream targets including those detected proteins that comprise the consensus panel described by Best et al. [13] among 47 LUAD cell lines. Columns are ranked (lowest to highest) by KYNU protein expression. **(D)** Scatter plot illustrating the association between CCLE-derived KYNU mRNA expression and a 10-gene NRF2 activation consensus signature described by Best et al. [13] among LUAD cell lines. A regression line and associated 95% confidence intervals is shown.



**Figure A3.** Association between KYNU and NRF2-gene based signatures in TCGA LUAD dataset. (A) Heatmap representing gene expression of NRF2-downstream targets including the consensus panel described by Best et al. [13] amongst TCGA LUAD tumors. Columns are ranked (lowest to highest) by KYNU mRNA expression. (B) Spearman correlation coefficients (95% confidence interval) between KYNU mRNA expression and the gene-based NRF2 consensus signature described by Best et al. [13] in TCGA-LUAD tumors stratified by presence or absence of *STK11* and *KEAP1* mutations. (C) Immunoblots for KYNU protein expression following siRNA-mediated knockdown of *STK11* in KYNU-low *STK11*-wild type LUAD cell lines H2009 and H3255. DF1024 and H2030 lysates were used as positive controls for KYNU protein expression.

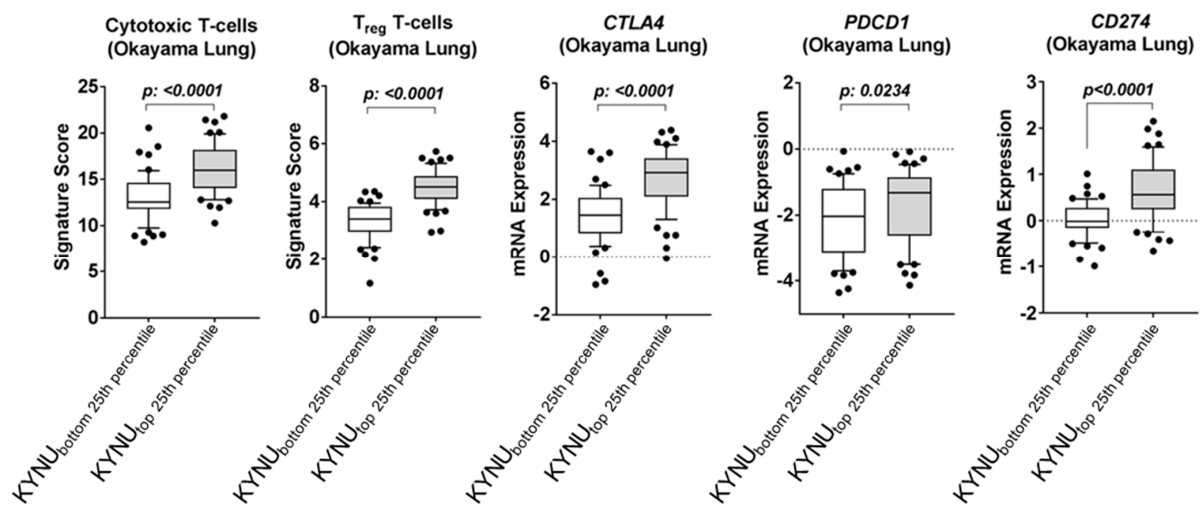


**Figure A4.** Association between *KYNU* mRNA expression and gene-based signatures of immune infiltrates and immune checkpoint blockade related genes. Box and whisker plots illustrating the distribution of gene-based signatures reflective of cytotoxic T-cells, regulatory T cells, as well as immune checkpoint blockade-related genes *CD274* (PDL-L1), *PDCD1* (PD1), and *CTLA4* in the Okayama Lung Cancer [24] gene expression dataset for LUAD tumors stratified by *KYNU* mRNA expression into the bottom and top 25th percentiles. The center line and bottom/upper bounds indicate median and 1st/3rd quartiles, respectively. Whiskers represent the 5th and 95th percentile of values. Statistical significance was determined by two-sided Wilcoxon rank sum test. Gene based signatures of immune infiltrates are based on Bindea et al. [36].

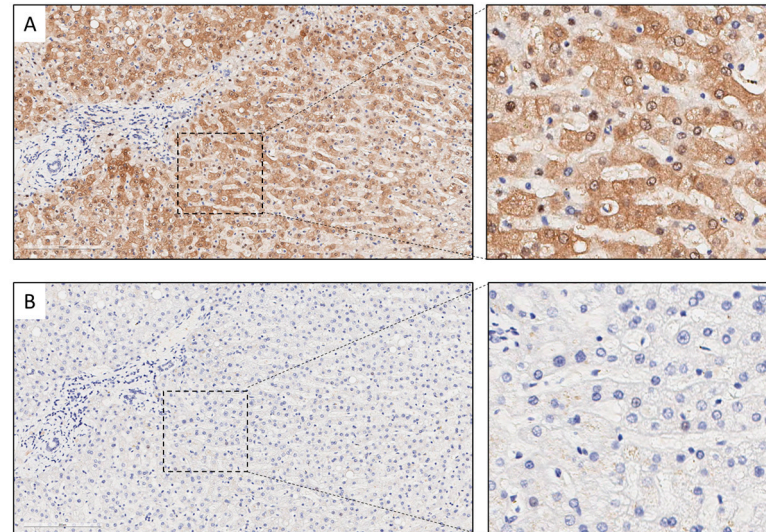


**Figure A5.** Microphotographs of immunohistochemistry staining of non-neoplastic liver control using *KYNU* antibody which shows positive cytoplasmic expression in hepatocytes (A), and diluent which displays negative expression of *KYNU* (B).

## References

- Best, S.A.; Ding, S.; Kersbergen, A.; Dong, X.; Song, J.Y.; Xie, Y.; Reljic, B.; Li, K.; Vince, J.E.; Rathi, V.; et al. Distinct initiating events underpin the immune and metabolic heterogeneity of *KRAS*-mutant lung adenocarcinoma. *Nat. Commun.* **2019**, *10*, 4190. [\[CrossRef\]](#)
- Okayama, H.; Kohno, T.; Ishii, Y.; Shimada, Y.; Shiraishi, K.; Iwakawa, R.; Furuta, K.; Tsuta, K.; Shibata, T.; Yamamoto, S.; et al. Identification of genes upregulated in *ALK*-positive and *EGFR/KRAS/ALK*-negative lung adenocarcinomas. *Cancer Res.* **2012**, *72*, 100–111. [\[CrossRef\]](#)

3. Bindea, G.; Mlecnik, B.; Tosolini, M.; Kirilovsky, A.; Waldner, M.; Obenauf, A.C.; Angell, H.; Fredriksen, T.; Lafontaine, L.; Berger, A.; et al. Spatiotemporal dynamics of intratumoral immune cells reveal the immune landscape in human cancer. *Immunity* **2013**, *39*, 782–795. [[CrossRef](#)]
4. Comprehensive molecular profiling of lung adenocarcinoma. *Nature* **2014**, *511*, 543–550. [[CrossRef](#)]
5. Skoulidis, F.; Byers, L.A.; Diao, L.; Papadimitrakopoulou, V.A.; Tong, P.; Izzo, J.; Behrens, C.; Kadara, H.; Parra, E.R.; Canales, J.R.; et al. Co-occurring genomic alterations define major subsets of KRAS-mutant lung adenocarcinoma with distinct biology, immune profiles, and therapeutic vulnerabilities. *Cancer Discov.* **2015**, *5*, 860–877. [[CrossRef](#)]
6. Kansanen, E.; Kuosmanen, S.M.; Leinonen, H.; Levonen, A.L. The Keap1-Nrf2 pathway: Mechanisms of activation and dysregulation in cancer. *Redox Biol.* **2013**, *1*, 45–49. [[CrossRef](#)]
7. Rojo de la Vega, M.; Chapman, E.; Zhang, D.D. NRF2 and the Hallmarks of Cancer. *Cancer Cell* **2018**, *34*, 21–43. [[CrossRef](#)]
8. Jeong, Y.; Hellyer, J.A.; Stehr, H.; Hoang, N.T.; Niu, X.; Das, M.; Padda, S.K.; Ramchandran, K.; Neal, J.W.; Wakelee, H.; et al. Role of KEAP1/NFE2L2 Mutations in the Chemotherapeutic Response of Patients with Non-Small Cell Lung Cancer. *Clin. Cancer Res.* **2020**, *26*, 274–281. [[CrossRef](#)]
9. Goeman, F.; De Nicola, F.; Scalera, S.; Sperati, F.; Gallo, E.; Ciuffreda, L.; Pallocca, M.; Pizzuti, L.; Krasniqi, E.; Barchiesi, G.; et al. Mutations in the KEAP1-NFE2L2 Pathway Define a Molecular Subset of Rapidly Progressing Lung Adenocarcinoma. *J. Thorac. Oncol.* **2019**, *14*, 1924–1934. [[CrossRef](#)]
10. Tanaka, Y.; Hamada, S.; Matsumoto, R.; Taguchi, K.; Yamamoto, M.; Masamune, A. Nrf2 expression in pancreatic stellate cells promotes progression of cancer. *Am. J. Physiol. Gastrointest. Liver Physiol.* **2021**, *321*, G378–G388. [[CrossRef](#)]
11. Sporn, M.B.; Liby, K.T. NRF2 and cancer: The good, the bad and the importance of context. *Nat. Rev. Cancer* **2012**, *12*, 564–571. [[CrossRef](#)]
12. Shibata, T.; Ohta, T.; Tong, K.I.; Kokubu, A.; Odogawa, R.; Tsuta, K.; Asamura, H.; Yamamoto, M.; Hirohashi, S. Cancer related mutations in NRF2 impair its recognition by Keap1-Cul3 E3 ligase and promote malignancy. *Proc. Natl. Acad. Sci. USA* **2008**, *105*, 13568–13573. [[CrossRef](#)]
13. Cykowiak, M.; Krajka-Kuźniak, V. Role of Nrf2 in Pancreatic Cancer. *Antioxidants* **2021**, *11*, 98. [[CrossRef](#)]
14. Tossetta, G.; Fantone, S.; Montanari, E.; Marzioni, D.; Goteri, G. Role of NRF2 in Ovarian Cancer. *Antioxidants* **2022**, *11*, 663. [[CrossRef](#)]
15. Best, S.A.; De Souza, D.P.; Kersbergen, A.; Policheni, A.N.; Dayalan, S.; Tull, D.; Rathi, V.; Gray, D.H.; Ritchie, M.E.; McConville, M.J.; et al. Synergy between the KEAP1/NRF2 and PI3K Pathways Drives Non-Small-Cell Lung Cancer with an Altered Immune Microenvironment. *Cell Metab.* **2018**, *27*, 935–943.e934. [[CrossRef](#)]
16. Galan-Cobo, A.; Sithideatphaiboon, P.; Qu, X.; Poteete, A.; Pisegna, M.A.; Tong, P.; Chen, P.H.; Boroughs, L.K.; Rodriguez, M.L.M.; Zhang, W.; et al. LKB1 and KEAP1/NRF2 Pathways Cooperatively Promote Metabolic Reprogramming with Enhanced Glutamine Dependence in KRAS-Mutant Lung Adenocarcinoma. *Cancer Res.* **2019**, *79*, 3251–3267. [[CrossRef](#)]
17. DeNicola, G.M.; Chen, P.H.; Mullarky, E.; Sudderth, J.A.; Hu, Z.; Wu, D.; Tang, H.; Xie, Y.; Asara, J.M.; Huffman, K.E.; et al. NRF2 regulates serine biosynthesis in non-small cell lung cancer. *Nat. Genet.* **2015**, *47*, 1475–1481. [[CrossRef](#)]
18. Mukhopadhyay, S.; Vander Heiden, M.G.; McCormick, F. The Metabolic Landscape of RAS-Driven Cancers from biology to therapy. *Nat. Cancer* **2021**, *2*, 271–283. [[CrossRef](#)]
19. Romero, R.; Sayin, V.I.; Davidson, S.M.; Bauer, M.R.; Singh, S.X.; LeBoeuf, S.E.; Karakousi, T.R.; Ellis, D.C.; Bhutkar, A.; Sánchez-Rivera, F.J.; et al. Keap1 loss promotes Kras-driven lung cancer and results in dependence on glutaminolysis. *Nat. Med.* **2017**, *23*, 1362–1368. [[CrossRef](#)]
20. Sayin, V.I.; LeBoeuf, S.E.; Singh, S.X.; Davidson, S.M.; Biancur, D.; Guzelhan, B.S.; Alvarez, S.W.; Wu, W.L.; Karakousi, T.R.; Zavitsanou, A.M.; et al. Activation of the NRF2 antioxidant program generates an imbalance in central carbon metabolism in cancer. *Elife* **2017**, *6*. [[CrossRef](#)]
21. Phillips, R.S. Structure and mechanism of kynureninase. *Arch. Biochem. Biophys.* **2014**, *544*, 69–74. [[CrossRef](#)] [[PubMed](#)]
22. Triplett, T.A.; Garrison, K.C.; Marshall, N.; Donkor, M.; Blazek, J.; Lamb, C.; Qerqez, A.; Dekker, J.D.; Tanno, Y.; Lu, W.C.; et al. Reversal of indoleamine 2,3-dioxygenase-mediated cancer immune suppression by systemic kynurenine depletion with a therapeutic enzyme. *Nat. Biotechnol.* **2018**, *36*, 758–764. [[CrossRef](#)] [[PubMed](#)]
23. Fahrman, J.F.; Bantis, L.E.; Capello, M.; Scelo, G.; Dennison, J.B.; Patel, N.; Murage, E.; Vykoukal, J.; Kundnani, D.L.; Foretova, L.; et al. A Plasma-Derived Protein-Metabolite Multiplexed Panel for Early-Stage Pancreatic Cancer. *J. Natl. Cancer Inst.* **2019**, *111*, 372–379. [[CrossRef](#)]
24. Fahrman, J.F.; Vykoukal, J.; Fleury, A.; Tripathi, S.; Dennison, J.B.; Murage, E.; Wang, P.; Yu, C.Y.; Capello, M.; Creighton, C.J.; et al. Association between plasma diacetylspermine and tumor spermine synthase with outcome in triple negative breast cancer. *J. Natl. Cancer Inst.* **2019**, *112*, 607–616. [[CrossRef](#)]
25. Gao, J.; Aksoy, B.A.; Dogrusoz, U.; Dresdner, G.; Gross, B.; Sumer, S.O.; Sun, Y.; Jacobsen, A.; Sinha, R.; Larsson, E.; et al. Integrative analysis of complex cancer genomics and clinical profiles using the cBioPortal. *Sci. Signal.* **2013**, *6*, p11. [[CrossRef](#)]
26. Rhodes, D.R.; Yu, J.; Shanker, K.; Deshpande, N.; Varambally, R.; Ghosh, D.; Barrette, T.; Pandey, A.; Chinnaiyan, A.M. ONCOMINE: A cancer microarray database and integrated data-mining platform. *Neoplasia* **2004**, *6*, 1–6. [[CrossRef](#)]

27. Parra, E.R.; Behrens, C.; Rodriguez-Canales, J.; Lin, H.; Mino, B.; Blando, J.; Zhang, J.; Gibbons, D.L.; Heymach, J.V.; Sepesi, B.; et al. Image Analysis-based Assessment of PD-L1 and Tumor-Associated Immune Cells Density Supports Distinct Intratumoral Microenvironment Groups in Non-small Cell Lung Carcinoma Patients. *Clin. Cancer Res.* **2016**, *22*, 6278–6289. [[CrossRef](#)]
28. Cecile Contal, J.O.Q. An application of changepoint methods in studying the effect of age on survival in breast cancer. *Comput. Stat. Data Anal.* **1999**, *30*, 253–270. [[CrossRef](#)]
29. Vykoukal, J.; Fahrman, J.F.; Gregg, J.R.; Tang, Z.; Basourakos, S.; Irajizad, E.; Park, S.; Yang, G.; Creighton, C.J.; Fleury, A.; et al. Caveolin-1-mediated sphingolipid oncometabolism underlies a metabolic vulnerability of prostate cancer. *Nat. Commun.* **2020**, *11*, 4279. [[CrossRef](#)]
30. Greulich, H. The genomics of lung adenocarcinoma: Opportunities for targeted therapies. *Genes Cancer* **2010**, *1*, 1200–1210. [[CrossRef](#)]
31. Frank, R.; Scheffler, M.; Merkelbach-Bruse, S.; Ihle, M.A.; Kron, A.; Rauer, M.; Ueckerth, F.; König, K.; Michels, S.; Fischer, R.; et al. Clinical and Pathological Characteristics of KEAP1- and NFE2L2-Mutated Non-Small Cell Lung Carcinoma (NSCLC). *Clin. Cancer Res.* **2018**, *24*, 3087–3096. [[CrossRef](#)] [[PubMed](#)]
32. Bryan, H.K.; Olayanju, A.; Goldring, C.E.; Park, B.K. The Nrf2 cell defence pathway: Keap1-dependent and -independent mechanisms of regulation. *Biochem. Pharmacol.* **2013**, *85*, 705–717. [[CrossRef](#)]
33. Opitz, C.A.; Wick, W.; Steinman, L.; Platten, M. Tryptophan degradation in autoimmune diseases. *Cell. Mol. Life Sci. CMLS* **2007**, *64*, 2542–2563. [[CrossRef](#)] [[PubMed](#)]
34. Mezrich, J.D.; Fechner, J.H.; Zhang, X.; Johnson, B.P.; Burlingham, W.J.; Bradfield, C.A. An interaction between kynurenine and the aryl hydrocarbon receptor can generate regulatory T cells. *J. Immunol.* **2010**, *185*, 3190–3198. [[CrossRef](#)] [[PubMed](#)]
35. Terness, P.; Bauer, T.M.; Rose, L.; Dufter, C.; Watzlik, A.; Simon, H.; Opelz, G. Inhibition of allogeneic T cell proliferation by indoleamine 2,3-dioxygenase-expressing dendritic cells: Mediation of suppression by tryptophan metabolites. *J. Exp. Med.* **2002**, *196*, 447–457. [[CrossRef](#)] [[PubMed](#)]
36. Heng, B.; Lim, C.K.; Lovejoy, D.B.; Bessede, A.; Gluch, L.; Guillemin, G.J. Understanding the role of the kynurenine pathway in human breast cancer immunobiology. *Oncotarget* **2015**, *7*, 6506–6520. [[CrossRef](#)] [[PubMed](#)]
37. Amobi, A.; Qian, F.; Lugade, A.A.; Odunsi, K. Tryptophan Catabolism and Cancer Immunotherapy Targeting IDO Mediated Immune Suppression. *Adv. Exp. Med. Biol.* **2017**, *1036*, 129–144. [[CrossRef](#)] [[PubMed](#)]
38. Fahrman, J.F.; Vykoukal, J.V.; Ostrin, E.J. Amino Acid Oncometabolism and Immunomodulation of the Tumor Microenvironment in Lung Cancer. *Front. Oncol.* **2020**, *10*, 276. [[CrossRef](#)]
39. Platten, M.; Wick, W.; Van den Eynde, B.J. Tryptophan catabolism in cancer: Beyond IDO and tryptophan depletion. *Cancer Res.* **2012**, *72*, 5435–5440. [[CrossRef](#)]
40. He, F.; Antonucci, L.; Karin, M. NRF2 as a regulator of cell metabolism and inflammation in cancer. *Carcinogenesis* **2020**, *41*, 405–416. [[CrossRef](#)]
41. Gwinn, D.M.; Lee, A.G.; Briones-Martin-del-Campo, M.; Conn, C.S.; Simpson, D.R.; Scott, A.I.; Le, A.; Cowan, T.M.; Ruggero, D.; Sweet-Cordero, E.A. Oncogenic KRAS Regulates Amino Acid Homeostasis and Asparagine Biosynthesis via ATF4 and Alters Sensitivity to L-Asparaginase. *Cancer Cell* **2018**, *33*, 91–107. [[CrossRef](#)] [[PubMed](#)]
42. Brunelli, L.; Caiola, E.; Marabese, M.; Broggin, M.; Pastorelli, R. Capturing the metabolomic diversity of KRAS mutants in non-small-cell lung cancer cells. *Oncotarget* **2014**, *5*, 4722–4731. [[CrossRef](#)] [[PubMed](#)]
43. Najumudeen, A.K.; Ceteci, F.; Fey, S.K.; Hamm, G.; Steven, R.T.; Hall, H.; Nikula, C.J.; Dexter, A.; Murta, T.; Race, A.M.; et al. The amino acid transporter SLC7A5 is required for efficient growth of KRAS-mutant colorectal cancer. *Nat. Genet.* **2021**, *53*, 16–26. [[CrossRef](#)] [[PubMed](#)]
44. Oh, M.H.; Sun, I.H.; Zhao, L.; Leone, R.D.; Sun, I.M.; Xu, W.; Collins, S.L.; Tam, A.J.; Blosser, R.L.; Patel, C.H.; et al. Targeting glutamine metabolism enhances tumor-specific immunity by modulating suppressive myeloid cells. *J. Clin. Investig.* **2020**, *130*, 3865–3884. [[CrossRef](#)]
45. Wu, W.C.; Sun, H.W.; Chen, J.; OuYang, H.Y.; Yu, X.J.; Chen, H.T.; Shuang, Z.Y.; Shi, M.; Wang, Z.; Zheng, L. Immunosuppressive Immature Myeloid Cell Generation Is Controlled by Glutamine Metabolism in Human Cancer. *Cancer Immunol. Res.* **2019**, *7*, 1605–1618. [[CrossRef](#)] [[PubMed](#)]
46. Carr, E.L.; Kelman, A.; Wu, G.S.; Gopaul, R.; Senkevitch, E.; Aghvanyan, A.; Turay, A.M.; Frauwirth, K.A. Glutamine uptake and metabolism are coordinately regulated by ERK/MAPK during T lymphocyte activation. *J. Immunol.* **2010**, *185*, 1037–1044. [[CrossRef](#)] [[PubMed](#)]
47. Wei, J.; Raynor, J.; Nguyen, T.-L.M.; Chi, H. Nutrient and Metabolic Sensing in T Cell Responses. *Front. Immunol.* **2017**, *8*, 247. [[CrossRef](#)]
48. Sonner, J.K.; Deumelandt, K.; Ott, M.; Thomé, C.M.; Rauschenbach, K.J.; Schulz, S.; Munteanu, B.; Mohapatra, S.; Adam, I.; Hofer, A.C.; et al. The stress kinase GCN2 does not mediate suppression of antitumor T cell responses by tryptophan catabolism in experimental melanomas. *Oncoimmunology* **2016**, *5*, e1240858. [[CrossRef](#)]
49. Quintana, F.J.; Sherr, D.H. Aryl hydrocarbon receptor control of adaptive immunity. *Pharmacol. Rev.* **2013**, *65*, 1148–1161. [[CrossRef](#)]
50. Mándi, Y.; Vécsei, L. The kynurenine system and immunoregulation. *J. Neural Transm.* **2012**, *119*, 197–209. [[CrossRef](#)]
51. Li, C.; Zhao, H. Tryptophan and Its Metabolites in Lung Cancer: Basic Functions and Clinical Significance. *Front. Oncol.* **2021**, *11*, 707277. [[CrossRef](#)] [[PubMed](#)]

52. Long, G.V.; Dummer, R.; Hamid, O.; Gajewski, T.F.; Caglevic, C.; Dalle, S.; Arance, A.; Carlino, M.S.; Grob, J.J.; Kim, T.M.; et al. Epcadostat plus pembrolizumab versus placebo plus pembrolizumab in patients with unresectable or metastatic melanoma (ECHO-301/KEYNOTE-252): A phase 3, randomised, double-blind study. *Lancet Oncol.* **2019**, *20*, 1083–1097. [[CrossRef](#)]
53. Weber, W.P.; Feder-Mengus, C.; Chiarugi, A.; Rosenthal, R.; Reschner, A.; Schumacher, R.; Zajac, P.; Misteli, H.; Frey, D.M.; Oertli, D.; et al. Differential effects of the tryptophan metabolite 3-hydroxyanthranilic acid on the proliferation of human CD8+ T cells induced by TCR triggering or homeostatic cytokines. *Eur. J. Immunol.* **2006**, *36*, 296–304. [[CrossRef](#)] [[PubMed](#)]
54. Yu, C.P.; Fu, S.F.; Chen, X.; Ye, J.; Ye, Y.; Kong, L.D.; Zhu, Z. The Clinicopathological and Prognostic Significance of IDO1 Expression in Human Solid Tumors: Evidence from a Systematic Review and Meta-Analysis. *Cell Physiol. Biochem.* **2018**, *49*, 134–143. [[CrossRef](#)]
55. Chuang, S.C.; Fanidi, A.; Ueland, P.M.; Relton, C.; Midttun, O.; Vollset, S.E.; Gunter, M.J.; Seckl, M.J.; Travis, R.C.; Wareham, N.; et al. Circulating biomarkers of tryptophan and the kynurenine pathway and lung cancer risk. *Cancer Epidemiol. Biomarkers Prev.* **2014**, *23*, 461–468. [[CrossRef](#)]
56. Wang, W.; Huang, L.; Jin, J.Y.; Pi, W.; Ellsworth, S.G.; Jolly, S.; Mellor, A.L.; Machtay, M.; Kong, F.S. A Validation Study on IDO Immune Biomarkers for Survival Prediction in Non-Small Cell Lung Cancer: Radiation Dose Fractionation Effect in Early-Stage Disease. *Clin. Cancer Res.* **2020**, *26*, 282–289. [[CrossRef](#)]
57. Wang, W.; Huang, L.; Jin, J.Y.; Jolly, S.; Zang, Y.; Wu, H.; Yan, L.; Pi, W.; Li, L.; Mellor, A.L.; et al. IDO Immune Status after Chemoradiation May Predict Survival in Lung Cancer Patients. *Cancer Res.* **2018**, *78*, 809–816. [[CrossRef](#)]
58. Karayama, M.; Masuda, J.; Mori, K.; Yasui, H.; Hozumi, H.; Suzuki, Y.; Furuhashi, K.; Fujisawa, T.; Enomoto, N.; Nakamura, Y.; et al. Comprehensive assessment of multiple tryptophan metabolites as potential biomarkers for immune checkpoint inhibitors in patients with non-small cell lung cancer. *Clin. Transl. Oncol.* **2020**, *23*, 418–423. [[CrossRef](#)]
59. Qian, Z.; Zhou, T.; Gurguis, C.I.; Xu, X.; Wen, Q.; Lv, J.; Fang, F.; Hecker, L.; Cress, A.E.; Natarajan, V.; et al. Nuclear factor, erythroid 2-like 2-associated molecular signature predicts lung cancer survival. *Sci. Rep.* **2015**, *5*, 16889. [[CrossRef](#)]
60. Arbour, K.C.; Jordan, E.; Kim, H.R.; Dienstag, J.; Yu, H.A.; Sanchez-Vega, F.; Lito, P.; Berger, M.; Solit, D.B.; Hellmann, M.; et al. Effects of Co-occurring Genomic Alterations on Outcomes in Patients with KRAS-Mutant Non-Small Cell Lung Cancer. *Clin. Cancer Res.* **2018**, *24*, 334–340. [[CrossRef](#)]